Author Manuscript

Author Manuscript

Author Manuscript

Author Manuscript

HHS Public Access

Author manuscript

Neuron. Author manuscript; available in PMC 2024 December 06.

Published in final edited form as:

Neuron. 2023 December 06; 111(23): 3819–3836.e8. doi:10.1016/j.neuron.2023.08.030.

Neuronal activity drives IGF2 expression from pericytes to form long-term memory

Kiran Pandey[1,2], **Benjamin Bessières**[1,2], **Susan L. Sheng**[1], **Julian Taranda**[3,4], **Pavel Osten**[3], **Ionel Sandovici**[5,6,7], **Miguel Constancia**[5,6,7], **Cristina M. Alberini**[1,*]

[1]Center for Neural Science, New York University, New York, NY, 10003, USA

[2]These authors contributed equally

[3]Cold Spring Harbor Laboratory, Cold Spring Harbor, New York, NY, 11724, USA

[4]current address: Neurology Clinic and National Center for Tumor Diseases, University Hospital; DKTK CCU Neurooncology, DKFZ, Heidelberg, 69120, Germany

[5]University of Cambridge Metabolic Research Laboratories and MRC Metabolic Diseases Unit, Institute of Metabolic Science, Addenbrookes Hospital, Cambridge, United Kingdom

[6]Department of Obstetrics and Gynaecology and National Institute for Health Research Cambridge Biomedical Research Centre, Cambridge, United Kingdom

[7]Centre for Trophoblast Research, Department of Physiology, Development and Neuroscience, University of Cambridge, Cambridge, United Kingdom

Summary

Investigations of memory mechanisms have been, thus far, neuron-centric, despite the brain comprises diverse cell types. Using rats and mice we assessed the cell type–specific contribution of hippocampal insulin-like growth factor 2 (IGF2), a polypeptide regulated by learning and required for long-term memory formation. The highest level of hippocampal IGF2 was detected in pericytes, the multi-functional mural cells of the microvessels that regulate blood flow, vessel formation, blood–brain barrier, and immune cell entry into the central nervous system. Learning significantly increased pericytic *Igf2* expression in the hippocampus, particularly in the highly vascularized *stratum lacunosum moleculare* and *stratum moleculare* layer of the dentate gyrus. *Igf2* increase required neuronal activity. Regulated hippocampal *Igf2* knockout in pericytes but not in fibroblasts or neurons impaired long-term memories and blunted the learning-dependent

*Lead contact and corresponding author: Cristina M. Alberini, Center for Neural Science, New York University, 4 Washington Place, New York, NY, 10003; ca60@nyu.edu; Phone: 212-998-7721.

Author contributions

K.P., B.B., S.L.S., J.T., P.O., C.M.A. designed the experiments. K.P., B.B., S.L.S., J.T. performed the experiments. M.C. and I.S. provided the Igf2-floxed mice. K.P., B.B., S.L.S., J.T. analyzed the data. C.M.A., K.P., B.B. S.L.S., wrote the article.

Publisher's Disclaimer: This is a PDF file of an unedited manuscript that has been accepted for publication. As a service to our customers we are providing this early version of the manuscript. The manuscript will undergo copyediting, typesetting, and review of the resulting proof before it is published in its final form. Please note that during the production process errors may be discovered which could affect the content, and all legal disclaimers that apply to the journal pertain.

Declaration of interests

The authors declare that no competing interests exist.

Author Manuscript Author Manuscript Author Manuscript Author Manuscript

increase of neuronal immediate early genes. Thus, neuronal activity-driven signaling from pericytes to neurons via IGF2 is essential for long-term memory.

E-TOC BLURB

Pandey, Bessieres et al. report that *Igf2* expression in hippocampal pericytes but not neurons, astrocytes, microglia, endothelial cells, or fibroblasts is increased by learning and required for long-term memory. Pericytic *Igf2* expression is driven by neuronal activity and controls neuronal mechanisms. Thus, pericyte-neuron cooperation plays a key role in memory.

Keywords

Insulin-like growth factor 2; pericyte; fibroblast; neuron; long-term memory; rat; mouse; hippocampus; immediate early gene; neuronal activity

Introduction

Insulin like growth factor 2 (IGF2 or IGFII) is a small protein that is upregulated in the hippocampus following learning and required for long-term memory formation[1]. The specific source of the hippocampal IGF2 that is critical for memory formation remains to be determined. In adult mammals, IGF2 is synthesized by the liver and choroid plexus but is also found in several other tissues including the brain stroma[2]. Endogenous *Igf2* mRNA levels in the rat dorsal hippocampus (dHC) increase following episodic learning, and injection of antisense oligodeoxynucleotides (AS-ODN) against IGF2 into the dHC disrupts the formation of long-term memory[1], suggesting that the synthesis of IGF2 critical for long-term memory takes place in cells of the hippocampal stroma. The identity of these cells, however, remains unknown.

Investigations of the biological bases of memory formation have thus far focused mainly on neurons and neuronal networks. Likewise, the development of new research technologies and computational modeling aiming at elucidating the biology of cognitive functions, including memory, has been strongly neuron-centric. However, memory is a function of the brain working as a system, i.e., a complex tissue comprising many cell types in multiple brain regions. The cell types that constitute the brain include neurons, various subpopulations of glial cells, and a well-regulated system of vasculature formed by endothelial cells, pericytes, and smooth muscle cells, and fibroblasts in the perivascular space. Together, these cell populations form a neurovascular tissue that supports brain functions[3,4]. Coordinated communication among neurons, glial, and vascular cells is required for the regulation of cerebral blood flow, which ensures that blood supply is tightly matched with the metabolic demand of the brain—a process known as “neurovascular coupling”[3,5].

In this study, we assessed the cell type–specific expression of IGF2 in the dHC of rats and mice and found that its highest expression occurs in pericytes and fibroblasts. We also found that learning significantly increases *Igf2* in pericytes but not in neurons, astrocytes or fibroblasts. The pericytic *Igf2* increase required neuronal activity. The regulated deletion of

Author Manuscript Author Manuscript Author Manuscript Author Manuscript

Igf2 in pericytes, and particularly in hippocampal pericytes, but not in fibroblasts or neurons, impaired long-term memory without affecting short-term memory. Pericytic IGF2 ablation also blocked the learning-dependent increase of immediate early genes (IEGs) in neurons. Therefore, our data provide evidence for a fundamental role of hippocampal pericytes and their cooperation with neurons in long-term memory.

Results

Expression of *Igf2* in the hippocampus is highly enriched in vascular cells, where it is induced by learning

By using RNAscope fluorescence *in situ* hybridization and confocal microscopy[6], we compared *Igf2* mRNA concentrations in various rat dHC subregions and cell types. RNAscope signal is revealed as a punctate staining, and previous studies demonstrated that each punctum corresponds to one molecule of the intended target mRNA. Hence, quantification of the number of puncta per cell offers a direct measurement of expression levels of a certain target[7].

Previous northern and western blot data reported that IGF2 mRNA and protein level, respectively, significantly increases in the dHC of rat 20 hours (h) following inhibitory avoidance (IA) learning[1]. The training-dependent increase at the protein level was shown to be selective for associative learning as unpaired control rats (exposed to the context and one hour later to the footshock in a different context) did not exhibit any IGF2 change relative to untrained (naïve) animals[1]. This non-associative context and shock experience does not elicit IA memory, thus controlling for non-associative effects[1]. Here we employed quantitative polymerase chain reaction (qPCR) to confirm whether training increases the dorsal hippocampal levels of *Igf2* mRNA at 20 h after IA training relative to untrained and unpaired control conditions. We found that training significantly increased *Igf2* mRNA levels relative to both untrained and unpaired conditions, whereas no *Igf2* difference was detected in the unpaired relative to the untrained controls (Figure S1A).

Next, we validated the *Igf2* RNAscope technique by including the choroid plexus, a structure known to highly express *Igf2*[2] (Figure S1B). We also performed a relative quantification analysis of *Igf2* mRNA in the dHC subregions of rats (Figure 1A); we found that, relative to the CA1, CA3 and dentate gyrus (DG) subregions, the area of the *stratum lacunosum moleculare* and the *stratum moleculare* layer of the upper blade of the DG had significantly more *Igf2* mRNA puncta (Figure 1A; also see Figure S1C,D for larger panels and higher magnification images). *Igf2* puncta were associated with markers of excitatory (CamKIIα) and inhibitory (Gad1) neurons, astrocytes (Aldh1l1), and vascular cells (Pecam1) (Figure 1B; also see Figure S1E for larger panels and higher magnification images), but vascular cells had by far the highest number of *Igf2* puncta (Figure 1B).

Because *Igf2* mRNA levels significantly increased in the rat dHC 20 h following IA learning[1,8], we employed the same species and learning paradigm combined with RNAscope to assess the learning-dependent, cell type-specific changes in *Igf2* expression. We found that *Igf2* mRNA levels increase significantly in the CA1 and SLM subregions following training (Figure 1C). We observed that 30–40% of cells in each dHC subregion (CA1, CA3,

Author Manuscript Author Manuscript Author Manuscript Author Manuscript

DG, and SLM) expressed *Igf2*; while this proportion did not change following training (Figure 1D), a significant increase in the number of *Igf2* mRNA puncta was detected in vascular cells, but not in excitatory or inhibitory neurons, or astrocytes of the CA1, SLM (Figure 1E, F), and DG (Figure S1G) subregions. *Igf2* mRNA puncta did not change after training in CA3 vasculature cells (Figure S1F). We concluded that the significant *Igf2* induction elicited by learning mainly takes place in vascular cells.

Igf2 is highly expressed in pericytes where it is upregulated following learning

To more clearly identify which types of brain vascular cells express *Igf2* mRNA, we employed RNAscope in combination with immunohistochemical staining. The vascular cell types of the brain include endothelial cells, pericytes, astrocytes, and smooth muscle cells[9]. Because astrocytes had low levels of *Ig2* mRNA (Figure 1B), we assessed the colocalization of *Igf2* mRNA with *Lycopersicon esculentum* agglutinin, a tomato lectin protein (hereafter lectin) that labels vascular endothelial cells[10]. We also determined the colocalization of *Igf2* with platelet derived growth factor receptor-beta (PDGFRB), a protein highly expressed in pericytes, but also present in smooth muscle cells and fibroblasts[11] (Figure 1G, H; also see Figure S2A). Fluorescence intensity analyses revealed that 34±7% of *Igf2* puncta colocalized with PDGFRB, while only 2.3 ± 0.3% of *Igf2* puncta colocalized with lectin (Figure 1H). The remaining 63.8 ± 7.3% of *Igf2* puncta could not be assigned to either cell type (undetermined) due to their intertwined histological organization and the limitations of imaging resolution (Figure 1H). The cell type distribution of *Igf2* did not change significantly following training (Figure 1H).

Next, we employed mice to better define the cell type expression of *Igf2* in vascular cells and other cell types by using fluorescence activated cell sorting (FACS). One advantage of transitioning to mice was the availability of mouse genetic tools for behavioral testing. The experiments across species and hippocampus-dependent learning paradigms also provided validation of the fundamental role of Igf2 in memory formation. We isolated cell populations enriched in pericytes or endothelial cells from the mouse dHC using, respectively, an anti-CD13 antibody, which targets a zinc metallopeptidase expressed on pericytes[12] and an anti-CD31 antibody, which recognizes a glycoprotein also known as platelet endothelial cell adhesion molecule (PECAM-1) that is expressed by endothelial cells[13]. We confirmed the enrichment of pericytic and endothelial cell populations by performing qPCR on the RNAs isolated from the sorted cell population RNAs using two pericytic markers, the *Pdgfrb* and ATP binding cassette subfamily C member 9 (*Abcc9*, an ATP-binding cassette transporter[14]), and the endothelial marker solute carrier family 2 member 1 (*Slc2a1*, also known as *Glut1*[15]). The results validated the cell population sorting as they confirmed that the CD13+ and CD31+ cells selectively expressed the pericyte or endothelial cell markers, respectively (Figures 2A, B).

QPCR for *Igf2* mRNA using two distinct sets of primers revealed that the level of *Igf2* was 5–7 fold enriched in the CD13+ cells (pericyte marker) compared to total dHC, but it was negligible in CD31+ cells (endothelial cell marker) (Figure 2C).

To further determine which cell populations express *Igf2* and their learning-dependent regulation, we investigated additional cell-specific markers. In the central nervous system,

Author Manuscript Author Manuscript Author Manuscript Author Manuscript

PDGFRB is highly expressed in pericytes but also in smooth muscle cells and fibroblasts found in the meninges and perivascular space[16,17]. To dissect which of these cell populations express *Igf2*, we used qPCR to quantify *Igf2* mRNA levels in FACS-purified hippocampal CD13+ cells (pericytes) and collagen type I alpha 1 chain (COL1A1)+ cells (fibroblasts)[17] (Figure 2D). We assessed these markers in untrained conditions and 20 h following contextual fear conditioning (CFC), an aversive, hippocampus-dependent, contextual learning. The timepoint of 20 h after learning was chosen based on rat IA studies showing that Igf2 mRNA and protein levels significantly increase 20 h post-training[1]. Western blot confirmed that IGF2 significantly increases 20 h after CFC in the dHC of mice (Figure S2B). Furthermore, the FACS purified cell population using anti-CD13 was validated as pericytes based on high enrichment of two other markers of pericytes, *Abcc9* and *Pdgfrb* (see Figures 2A and 2D), relatively low levels of markers of endothelial cells i.e, *Slc2a1* (see Figure 2B) and of fibroblasts, i.e., *Col1a1* (see Figure 2D). This array of markers supported the conclusion that the CD13+ cells were highly enriched in pericytes and not in fibroblasts.

FACS with CD13 and COL1A1 antibodies followed by qPCR showed that the two cell populations have similar levels of *Igf2* mRNA in untrained conditions. However, only the CD13+ cells had a significant increase in the level of *Igf2* mRNA after CFC training (Figure 2D). The levels of *Pdgfrb* and *Col1a1* did not change following training in either cell population (Figure 2D). The *Igf2* mRNA increase in CD13+ cells did not occur in control mice that received an immediate shock (IS) relative to untrained conditions (for IS see methods), a procedure that does not elicit an associative contextual fear memory and therefore controls for non-associative behavioral effects[18] (Figure 2E). *Pdgfrb* mRNA levels did not change across groups of CD13+ isolated cells, validating the increase in *Igf2* mRNA with training (Figure 2E).

To determine whether the learning-dependent increase in pericytic *Igf2* requires neuronal activity, we bilaterally injected the dHC of mice with an adeno-associated virus (AAV) expressing the inhibitory Designer Receptor Exclusively Activated by Designer Drugs (DREADDs) hM4Di along with the fluorescent reporter mCherry under the human synapsin (hSyn) neuronal promoter (AAV-hSyn-hM4Di-mCherry). To silence neuronal activity in the dHC, two weeks after viral injection, the mice were injected intraperitoneally (*i.p.*) with either vehicle (VEH) or compound 21 (C21, a ligand that activates the hM4Di receptor[19]) 30 minutes (min) before CFC. Control groups of mice received AAV expressing only mCherry (AAV-hSyn-mCherry) and were injected *i.p.* with vehicle or C21 to control for off-target effects. As shown in Figure S2C, C21 injection in hM4Di-expressing mice, but not in controls, impaired CFC memory at 1 day after training.

In parallel groups of mice that underwent similar treatments *Igf2* mRNA level was determined 20 h after CFC in RNA extracts obtained from the whole dHC (total) and dHC CD13+ cells (pericytes) enriched via FACS. *Igf2* level was significantly increased in vehicle-injected trained mice relative to vehicle-injected untrained controls, both in the total as well as CD13+ cell extracts (Figure 2F). Chemogenetic inhibition of neuronal activity with C21 completely blocked the increase of *Igf2* mRNA in both total and CD13+ cell extracts (Figure 2F). The levels of *Pdgfrb*, which were enriched in CD13+ cells, did not

Author Manuscript Author Manuscript Author Manuscript Author Manuscript

change with training in any of the groups (Figure S2D). Collectively, these data suggest that the learning-induced increase in pericytic *Igf2* requires neuronal activity.

The contribution of pericytes to brain functions is still poorly understood. Pericytes, which are vascular mural cells located at the abluminal surface of microvessels, are embedded in a common basement membrane with endothelial cells in blood microvessels, a site of the blood-brain barrier (BBB)[20]. Thus, pericytes are uniquely positioned within the neurovascular unit to communicate with endothelial cells, astrocytes, and neurons[21]. These cellular communications are believed to regulate neurovascular functions including BBB formation and maintenance, vascular stability and angioarchitecture, capillary blood flow, clearance of toxins, and acquisition of stem cell–like properties[19,22,23]. Recent studies showed that pericytes play important roles in a wide range of diseases that are characterized by cognitive impairments such as cerebral small vessel disease, acute stroke, Alzheimer's disease, and other neurological disorders[23–25]. Yet, the role of pericytes in healthy cognitive functions remains unknown.

In order to further characterize the selective expression and learning-dependent upregulation of IGF2 in pericytes we employed an *Igf2*-reporter mouse that carries a knock-in of histone H2B in tandem with the fluorescent protein tdTomato downstream of the endogenous *Igf2* promoter (tdTomato-H2B) (Figure 3A). By assessing the tdTomato fluorescence targeted to the nucleus via H2B, we therefore quantified the distribution of *Igf2*–expressing cells. As expected, the tdTomato fluorescent signal in the *Igf2*-reporter mouse brain was highly expressed in choroid plexus and leptomeninges (Figure S3A). Consistent with the RNAscope analysis in rats, the total number of cells (tdTomato-positive nuclei) in the dHC of mice did not change with CFC training (Figure 3B); however, the intensity of tdTomato fluorescence increased significantly, as revealed by a shift in the cumulative frequency distribution of tdTomato fluorescence (Figure 3C) with a significant increase particularly in the low-fluorescence intensity cell population (Figure 3D). The quantifications of the number of tdTomato positive nuclei in the dHC subregions revealed a significant increase following CFC training in CA1 and SLM/*stratum moleculare* layer of DG (Figure 3E).

Because in rats SLM had the highest level of *Igf2*, we quantified the number of tdTomato positive cells that co-expressed markers of pericytes, endothelial cells, fibroblasts, or microglia in the SLM subregion of mice. Double staining immunohistochemical analysis of tdTomato with PDGFRB or CD31 revealed that *Igf2* in the vasculature is found in pericytes and not in endothelial cells (Figure 3F, G, also see Figure S3B, C). These results were also confirmed by the "bump on a log" morphology of the tdTomato/PDGFRB staining, which is typical of pericytes[26] (Figure 3F, also see Figure S3B, C). Specifically, in untrained mice, 92.7 ± 5.6% of tdTomato-labeled nuclei colocalized with the pericytic marker PDGFRB (Figure 3F). This colocalization increased slightly following training, to 97.7 ± 1.1%, although the effect was not statistically significant (Figure S3C). The remaining 7.4 ± 5.6% of tdTomato-positive cells in untrained mice and 2.3 ± 1.1% of tdTomato positive cells in trained mice could not be assigned to any cell-type identity, as they did not clearly colocalize with either PDGFRB or CD31 (Figure S3C), possibly due to imaging limitations or the orientation of cells within the tissue section.

Author Manuscript Author Manuscript Author Manuscript Author Manuscript

Furthermore, in the SLM/*stratum moleculare* layer of DG, the number of tdTomato positive nuclei significantly increased following CFC (Figure S4A) and did not colocalize with the fibroblast marker COL1A1 in either untrained conditions or following CFC training (Figure 3H and S4A). Finally, tdTomato-labeled nuclei did not colocalize with cells labeled with the microglia marker ionized calcium binding adaptor molecule 1 (IBA1, also known as Allograft inflammatory factor 1[27]) (Figure 3I; also see Figure S4B) in any dHC subregions in either untrained controls or following CFC training [IBA1+/tdTomato+ cells in untrained: 7.0 ± 1.7% of in CA1, 4.3 ± 1.8% in CA3, 7.5 ± 1.7% in DG, and 5.5 ± 1.4% in SLM/*stratum moleculare* layer of DG; in trained: 5.0 ± 1.9% in CA1, 4.5 ± 1.7% in CA3, 6.0 ± 1.8% in DG, and 5.5 ± 1.5% in SLM (Figure S4B)].

In sum, the *Igf2*-reporter mouse, like wild-type rats and mice, showed that dHC *Igf2* expression is higher in vasculature cells and particularly in pericytes, relative to endothelial cells. Pericytic *Igf2* was significantly upregulated following CFC learning. Furthermore, dHC fibroblasts expressed *Igf2* but learning did not change *Igf2* level. The expression level of *Igf2* was low in microglia and it did not change following learning.

IGF2 in pericytes is required for long-term memory formation

We next proceeded to test the functional contribution of cell type-specific expression of *Igf2* in memory formation.

Given the selective pericytic upregulation of *Igf2* following training, we started by targeting pericytes. For this purpose, we generated a mouse line harboring an inducible knockout of *Igf2* in pericytes by crossing mice carrying *loxP* sites flanking exons 4–6 of *Igf2*[28,29] with mice expressing the Cre-ER^{T2} recombinase under the control of the pericyte murine *Pdgfrb* promoter (PDGFRB-P2A-CreER^{T2} [30]) (Figure 4A).

Induction of the knockout by *i.p.* injections of tamoxifen (TAM, 40 mg/kg) once a day for 5 consecutive days significantly decreased *Igf2* levels in the pericytes of Igf2$^{flox/flox}$/PDGFRB-P2A-CreER$^{T2+/-}$ mice (Igf2/Peri-KO) relative to the pericytes of vehicle-injected Igf2$^{flox/flox}$/PDGFRB-P2A-CreER$^{T2+/-}$ mice (Igf2/Peri-Control) (Figure 4B). The selective decrease of *Igf2* in pericytes was shown by qPCR quantification of *Abcc9, Slc2a1, Col1a1*, and *Igf2* in FACS-purified cell populations obtained with anti-CD13 (pericytes), anti-CD31 (endothelial cells), and anti-COL1A1 (fibroblasts) derived from dHC of mice (Figure 4B). As shown in Figure 4B, *Igf2* level was knocked down by 98% in CD13+ cells two weeks after tamoxifen treatment in Igf2/Peri-KO mice relative to Igf2/Peri-Control; in contrast, the levels of *Igf2* in CD31+ and COL1A1+ cells remained unchanged. In addition, the levels of the control markers *Actb* and *Gapdh* did not change in the RNA extracts from the whole dHC or from CD13+ cells obtained from either Igf2/Peri-KO or Igf2/Peri-Control mice (Figure S4C).

Notably, the selective knockdown of pericytic *Igf2* led to a small but significant increase in vascular and/or BBB permeability of the dHC, as shown by extravasation of Evans Blue dye in dHC (Figure S5A). However, learning did not affect the level of extravasation of Evans Blue dye in dHC (Figure S5B) and the pericytic *Igf2* knockdown did not change the number of dHC PDGFRB+ cells (Figure S5C).

Author Manuscript Author Manuscript Author Manuscript Author Manuscript

We next examined the effect of pericyte-specific *Igf2* knockout on memory formation using novel object location (nOL) and CFC, two hippocampus-dependent tasks that model spatial and contextual types of memory, respectively[31,32]. To this end, we performed sequential behavioral assessments starting with open field, which measures locomotor activity and anxiety behavior[33], followed, 2 days later, by nOL and 7 days later by CFC (Figure 4C). For these behavioral experiments, in addition to Igf2/Peri-Control and Igf2/Peri-KO mice, we added another control group, which consisted in $Igf2^{flox/flox}$ mice injected with tamoxifen (Igf2/NoCre-TAM), to account for the effect of tamoxifen injections.

We observed no significant difference in velocity, distance traveled, or time spent in the open field arena center between Igf2/Peri-Control, Igf2/Peri-KO mice or Igf2/NoCre-TAM (Figure 4D). In contrast, in comparison with the Igf2/Peri-Control and Igf2/NoCre-TAM groups, Igf2/Peri-KO mice were significantly impaired in long-term nOL memory tested 4 hours post-training (Figure 4E). Short-term nOL memory, tested 5 minutes after learning (Figure 4E), was not affected, indicating that pericytic IGF2 is required for memory consolidation but not for learning or short-term memory. No effect was observed on the total object exploration times in all groups (Figure 4E), supporting the conclusion that the impairment at 4 h post-training was indeed due to memory disruption. Similarly, compared to Igf2/Peri-Control and Igf2/NoCre-TAM mice, Igf2/Peri-KO mice had normal short-term CFC memory 1 h after training (Figure 4F) but a significant impairment in long-term CFC memory at 1 or 7 days after training (Figure 4F). To verify that the persistence in memory impairment at 7 days after training was not the result of the previous testing (for example an effect of extinction), an independent experiment was conducted in which Igf2/Peri-KO mice were tested only at 7 days after CFC training. The results confirmed that Igf2/Peri-KO mice had an impaired long-term memory (Figure S6A, B).

Knockout of *Igf2* in dHC pericytes impairs long-term memory formation

To test whether IGF2 derived from pericytes of the dHC plays a role in long-term memory formation, $Igf2^{flox/flox}$/PDGFRB-P2A-$CreER^{T2+/-}$ mice and control $Igf2^{flox/flox}$ mice were injected with 4-hydroxytamoxifen (4-OHT) (dHC-Igf2/Peri-KO and dHC-Igf2/NoCre-TAM, respectively) for 3 days into the dHC, and underwent behavioral testing 2 weeks later (Figure 5A). The dHC-Igf2/Peri-KO mice had a significant impairment in long-term nOL memory tested 4 hours post training (Figure 5B) as well as in long-term CFC memory tested at 1 and 7 days after training (Figure 5C), confirming that IGF2 derived from hippocampal pericytes is required for long-term memory formation. In addition, compared to dHC-Igf2/NoCre-TAM mice, dHC-Igf2/Peri-KO mice had normal short-term CFC memory, tested at 1 h after training (Figure S6C, D), indicating that dHC pericytic IGF2 is required for memory consolidation but not for learning or short-term memory. To confirm the selective knockout of *Igf2* in dHC pericytes, the dHC and primary somatosensory cortices (S1) of the mice as well as FACS-purified pericytes (CD13+) and endothelial cells (CD31+) from both regions underwent qPCR analyses to determine *Igf2* mRNA levels. As shown in Figures 5D and 5E, there was a significant decrease of pericytic *Igf2* mRNA in the dHC but not in S1 of dHC-Igf2/Peri-KO relative to dHC-Igf2/NoCre-TAM mice.

Author Manuscript Author Manuscript Author Manuscript Author Manuscript

Selective knockout of *Igf2* in fibroblasts or neurons did not affect memory formation

To determine whether selective deletion of *Igf2* in other cell types affect long-term memory formation, we induced *Igf2* knockout in fibroblasts or neurons of the dHC and tested the effects on contextual fear memory.

DHC injections of lentivirus expressing Cre-recombinase under *Col1a1* promoter significantly decreased *Igf2* levels in the COL1A1+ cell-sorted population, (i.e, fibroblasts) of $Igf2^{flox/flox}$ mice (dHC-Igf2/Fibro-KO or F-KO) relative to fibroblasts obtained from control mice ($Igf2^{flox/flox}$ mice that were injected with control lentivirus containing GFP under *Col1a1* promoter; dHC-Igf2/Fibro-Control or Con) (Figure 6A,B). This selective decrease of *Igf2* in fibroblasts was demonstrated by FACS of fibroblasts from the dHC of mice using an anti-Col1a1 antibody, and assessment by qPCR of *Col1a1, Pdgfrb*, and *Igf2* levels (Figure 6B). *Igf2* level was reduced by 86% in COL1A1+ cells of dHC-Igf2/Fibro-KO mice relative to dHC-Igf2/Fibro-Control. The level of *Igf2* did not change in the dHC total RNA extracts obtained from either dHC-Igf2/Fibro-KO or dHC-Igf2/Fibro-Control mice (Figure 6B). The knockout of *Igf2* in dHC COL1A1+ cells had no effect on CFC memory tested at 1 and 7 days after training (Figure 6C), indicating that IGF2 expressed by hippocampal fibroblasts does not play a critical role in long-term memory formation.

DHC injection of AAV expressing Cre-recombinase under hSyn promoter, which targets neuronal cells, decreased *Igf2* levels in NeuN+ FACS-purified cells, i.e., neurons, of dHC, obtained from $Igf2^{flox/flox}$ mice (dHC-Igf2/Neuro-KO or N-KO) relative to neuron of $Igf2^{flox/flox}$ mice injected with control AAV containing GFP under hSyn promoter (dHC-Igf2/Neuro-Control or Con) (Figure 6D and Figure S6E). Validation was performed using qPCR for *NeuN, Pdgfrb, Col1a1*, and *Igf2* (Figure 6D). *Igf2* level was decreased by 99% in NeuN+ cells of dHC-Igf2/Neuro-KO mice relative to dHC-Igf2/Neuro-Control. The *Igf2* level did not change in the dHC total RNA extracts obtained from either dHC-Igf2/Neuro-KO or dHC-Igf2/Neuro-Control mice (Figure 6D). Selective knockout of *Igf2* in dHC NeuN+ cells did not affect CFC memory tested at 1 and 7 days after training (Figure 6E), showing that IGF2 produced by hippocampal neurons is not critical for long-term memory formation.

Pericytic IGF2 is required for learning-dependent induction of neuronal immediate early genes

Given the selective pericytic role of IGF2 in memory, we next investigated whether IGF2 knockout in pericytes decreased the expression of IGF2 or changed the levels of IGF2 receptor (IGF2R, also known as cation-independent mannose-6-phosphate receptor or CIM6PR), and whether it affected neuronal activation mechanisms, such as the induction of IEGs evoked by learning[34]. Toward this end, we performed western blot analyses on dHC extracts obtained from Igf2/Peri-Control and Igf2/Peri-KO mice, untrained or trained in CFC, to measure the levels of pro-IGF2, IGF2, IGF2R, and of the IEGs ARC, FOS, and EGR1. Mice that underwent CFC were euthanized 1 h after training, an optimal timepoint for detecting learning dependent IEG induction[35]. Untrained control groups received either vehicle or tamoxifen injections, remained in the home cages, and were euthanized at matched time points.

Author Manuscript Author Manuscript Author Manuscript Author Manuscript

As expected for a pericyte-specific *Igf2* knockout, the levels of both pro-IGF2 and IGF2 protein were significantly reduced in the Igf2/Peri-KO mice (Figure 7A); however, the level of IGF2R was significantly upregulated (Figure 7B). The mechanism underlying this increase requires further investigation, but we speculate that it may reflect an attempt to compensate for the loss of IGF2 signal.

Igf2/Peri-Control mice trained in CFC exhibited the expected significant increase in the levels of ARC, FOS, and EGR1 (Figure 7C–F). This increase was completely blunted by pericytic knockdown of *Igf2* (Figure 7C–F, also see Figure S7), indicating that pericytic IGF2 is required for the induction of neuronal plasticity mechanisms evoked by learning. Thus, pericytic induction of IGF2 controls neuronal plasticity mechanisms required for long-term memory formation, underscoring the essential cooperation of vasculature and neuronal cells in the brain to support cognitive functions.

Discussion

Pericytes, a cell type still understudied, located on capillaries, play essential roles in microvascular functions[20,22,23]. Recent studies have implicated pericytes in several neurological diseases such as epilepsy, spinal cord injury, stroke, traumatic brain injury, diabetes, Huntington's disease, Alzheimer's disease, multiple sclerosis, and amyotrophic lateral sclerosis[23–25]; however, their roles in healthy cognitive functions were unknown. This study demonstrated the key role of pericytes and their functional cooperation with neurons in hippocampus-dependent long-term memory. It also revealed a novel mechanism of action of pericytes in brain functions, because it showed that, in addition to meeting the energy demands of the brain, pericytes interact with neurons via the neuropeptide IGF2.

Pericytic Igf2 seems to have a relatively selective role in long-term memory. In fact, despite a relative high level of *Igf2* in the dorsal hippocampus was detected also in fibroblasts, only pericytes increased *Igf2* expression following learning. Several other types of cells. i.e., neurons, astrocytes, endothelial cells, and microglia had low levels of Igf2 and did not significantly change it upon learning. Moreover, only pericytic *Igf2*, but not *Igf2* from fibroblasts or neurons, selectively contributed to long-term memory formation. Whether IGF2 engages other cell types of the brain, that were not yet investigated and whether the neuronal-pericytic-neuronal cooperation occurs in other brain regions remain to be understood. Another question that shall be investigated is whether specific subpopulations of pericytes *vs.* all are responsive to neuronal activity.

Our RNAscope and immunohistochemistry studies in rats and an *Igf2*-driven reporter mouse extend previous findings showing that IGF2 in adult rodent brain is expressed in endothelial and perivascular cells of the neuropil microvasculature, in addition to the known sites of high IGF2 expression choroid plexus and meninges[36–38]. Our data also agree with RNA-seq analyses showing that *Igf2* is expressed in pericytes in mice[39,40] and that IGF2 is expressed in human brain pericytes[41].

Igf2 expression was found enriched particularly in the pericytes of the area SLM/*stratum moleculare* of the DG, a layer close to the hippocampal fissure and DG, which connects

Author Manuscript Author Manuscript Author Manuscript Author Manuscript

the entorhinal cortex and the CA1 subregion and is crucial for many aspects of spatial and episodic memory[42]. These data suggest that vascular reactivity in this brain area might be particularly dynamic following hippocampus-dependent learning. Notably, the SLM is the first area to degenerate in Alzheimer's disease[43], a disease recently associated with disruption of pericyte functions[25]. IGF2 significantly ameliorates deficits in Alzheimer disease mouse models[44,45] and reverses aging-related memory impairment[46], a condition linked to BBB breakdown in the hippocampus[47], supporting the conclusion that pericytes in specific brain areas play important roles in cognitive functions. The SLM is an area of integration because it contains not only the terminals of fibers originating from layer III of the entorhinal cortex[48] but also from other brain areas, such as the nucleus reuniens of the midline thalamus[49], the amygdaloid complex[50], and the inferotemporal cortex[51]. Thus, the SLM and DG stratum moleculare are well positioned to serve as a control node for hippocampal network activations, and their pericytic regulation upon learning may exert critical control over the hippocampus-dependent memory system.

Pericytes are a heterogeneous cell population[20,52,53] whose pleiotropic functions are still poorly understood. Our studies raise several important questions on the specific source and functional contributions of pericytic IGF2. For example, further studies should seek to define whether IGF2 is expressed by all types of pericytes or by one or more subpopulations.

As IGF2 expressed by pericytes, and particularly by dHC pericytes, is required for contextual and spatial memories, and regulates neuronal changes elicited by learning, such as the induction of the IEGs ARC, FOS and EGR1, we conclude that a functional link between pericytes and neurons in support of cognitive functions must exist. The mechanisms underlying such link are unknown. As IGF2 acts in both an autocrine and paracrine manner[29,54], we speculate that IGF2 from pericytes may affect blood flow and/or angiogenesis via autocrine mechanisms or act paracrinally on IGF2 receptors expressed on neurons or other intermediate cell types, which in turn may regulate neuronal responses. In support of a possible role of pericytic IGF2 on blood flow regulation, our data showed that knockout of *Igf2* in pericytes increases vascular and/or BBB permeability, suggesting that IGF2 acts as metabolic provider and/or promoters of capillary health[54,55]. As increased permeability is linked to brain injury and inflammation, we also speculate that the learning-dependent production of IGF2 may exert protective or rebalancing effects on the changes evoked by experience. Identifying and characterizing these BBB/blood flow regulation mechanisms shall be an important next research step. Given the fact that *Igf2* knockout in pericytes affected memory consolidation but not learning, short-term memory, open field behavior or total object exploration, we conclude that IGF2 produced by pericytes provides an active BBB-dependent functional contribution to long-term memory, rather than playing a non-specific role. These BBB functions, together with neuronal effects, which likely occur via IGF2 receptor (IGF2R) (highly expressed by neurons[35]), may constitute a coordinated neurovascular response critical for memory formation.

IGF2, which is part of the complex insulin/IGF-system[56] and has been mainly studied for its role in development, is relatively poorly characterized, and particularly little is known about its roles in the brain. Previous studies from our lab identified the role of hippocampal IGF2 in memory consolidation and enhancement via the activation of

Author Manuscript Author Manuscript Author Manuscript Author Manuscript

IGF2R[1]. Through the activation of diverse types of receptors, IGF2 serves multiple and diverse functions in embryonic development, cell growth and carcinogenesis, memory, and neuroprotection[1,57–60]; further investigations are needed to determine whether distinct sources of IGF2 support distinct functions. The sources of IGF2 include liver, choroid plexus, and brain cells[2] among which, as indicated by this study, in the hippocampus pericytes are major contributors. Little is known about the selective contributions of the different IGF2 sources to various tissues and functions. Previous studies showed that supplying recombinant IGF2 either intracerebrally or systemically during learning or memory retrieval significantly increases memory strength and persistence[1,58,61,62] and reverses multiple core deficits of autism in mouse models[46,63] as well as in aging-related memory impairments[46]. Where tested, these effects were found to be mediated by the selective activation of IGF2R[1,46] whose expression was found highly enriched in neurons but not detected in astrocytes or microglia[35]. Together, these findings suggest that the IGF2/IGF2R pathway plays critical roles in the regulation of mechanisms and circuitry implicated in a variety of brain functions, whose underlying mechanisms of action however remain to be fully elucidated[64].

In sum, the results of this study underscore the importance of the cooperative outcome of the neurovascular brain tissue in cognitive functions. Further understanding of the regulation of IGF2 expression in pericytes, the mechanisms underlying the neuronal activity that drives IGF2 expression in pericytes, and the effects of pericytic IGF2 on neurons and cognitive functions is likely to contribute to the development of novel therapeutic approaches for neuropsychiatric diseases, including cognitive impairments and neurodegenerative diseases.

STAR Methods

Resource Availability

Lead contact: Further information and requests for resources and reagents should be directed to and will be fulfilled by the lead contact, Cristina M. Alberini (ca60@nyu.edu).

Materials availability: This study did not generate new unique reagents.

Data and code availability

- All data reported in this study will be shared by the lead contact upon request.
- This paper does not report original code.
- Any additional information required to reanalyze the data reported in this paper is available from the lead contact upon request.

Experimental Models and Subject Participant Details

Rats: Adult male Long-Evans rats weighing 200-250g were purchased from Envigo. Rats were group housed (2/cage) and maintained on a 12-hour light/dark cycle. Experiments were performed during the light cycle. All animals were allowed *ab libitum* access to food and water and were handled for 3 minutes per day for 5 days prior to any procedure. All protocols complied with the National Institutes of Health Guide for the Care and Use

Author Manuscript Author Manuscript Author Manuscript Author Manuscript

of Laboratory Animals and were approved by the New York University Animal Welfare Committee.

Mice: Adult male C57BL6 (stock 000664) and PDGFRB-P2A-Cre^{ERT2} (stock 030201)[30] mice were purchased from Jackson Laboratories. *Igf2*-floxed mice were generated and kindly provided by Drs. Miguel Constancia and Ionel Sandovici, University of Cambridge. These mice were described previously[28,29]. *Igf2*-floxed mice were bred in house and crossed with PDGFRB-P2A-Cre^{ERT2} mice (Jackson Laboratories, stock# 030201). Genotyping was conducted by Transnetyx (Memphis, TN). Both male and female mice were used in all experiments except for establishing cell sorting for pericytes and endothelial cells (Figure 2A) and confirming the learning-induced increase in IGF2 (Figure S2B). Mice were group housed (2-4/cage) and maintained on a 12-hour light/dark cycle. Experiments were performed during the light cycle. All animals were allowed *ab libitum* access to food and water and were handled for 3 minutes per day for 5 days prior to any procedure. For *Igf2* knockout in pericytes (PDGFRB-P2A-Cre^{ERT2}:IGF2$^{flox/flox}$ mice), Cre-recombinase activity was induced by *i.p.* injections of tamoxifen (Sigma) 40 mg/kg mouse/day in corn oil (Sigma) solution once a day for 5 consecutive days[65]. All protocols complied with the National Institutes of Health Guide for the Care and Use of Laboratory Animals and were approved by the New York University Animal Welfare Committee. Experiments with IGF2-tdTomato-H2B mice were conducted at Cold Spring Harbor Laboratories (CSHL); these experiments were approved by the Cold Spring Harbor Laboratory Animal Care and Use Committee. Animals were randomly assigned to treatment or behavioral groups for all experiments.

Method details

Inhibitory Avoidance (IA) and unpaired context and shock procedure (Un) in rats—IA was carried out as described previously[1]. The IA chamber (Med Associates. Inc., St. Albans, VT) consisted of a rectangular Perspex box divided into a safe compartment and a shock compartment. Foot shocks were delivered to the grid floor of the shock chamber via a constant current scrambler circuit. The apparatus was located in a sound-attenuated, non-illuminated room. During training sessions, each rat was placed in the safe (white, illuminated) compartment with its head facing away from the door. After 10 seconds (s), the door separating the compartments was automatically opened, allowing the rat access to the shock (black, dark) compartment. The door closed 1 second after the rat entered the shock compartment, and a brief foot shock (0.9 mA for 2 seconds) was administered. Controls consisted of rats that remained in their home cage (Untrained). Animals were euthanized 20 h after training and brain tissue was collected for biochemical or molecular assessments. The unpaired context and shock paradigm (Un) consisted of exposing rats first to the training context and, one hour later, to a foot shock in the same intensity as that received during training but delivered immediately after placing the rat on a grid. This unpaired exposure does not evoke IA memory[1].

Cannula implants and 4-OHT injections in mice—Mice were anesthetized with ketamine (75 mg/kg) mixed with xylazine (10 mg/kg), and stainless-steel guide cannulas (C313GS-5/SP; 22-gauge, P Technologies, Roanoke, VA) were implanted bilaterally using

Author Manuscript Author Manuscript Author Manuscript Author Manuscript

a stereotaxic apparatus (Kopf Instruments, Tujunga, CA) through holes drilled in the overlying skull to target the dHC (−2.0 mm anterior, ±1.4 mm lateral, −0.8 mm ventral from bregma). The guide cannulas were fixed to the skull with dental cement. At the end of the surgery, mice were administered meloxicam (3 mg/kg, subcutaneous) and let recover for 14 days before undergoing prior to further experimental manipulations. 4-hydroxytamoxifen (4-OHT; Sigma, H6278) was dissolved at 20 mg/ml in ethanol by shaking at 37°C for 30 minutes and was then aliquoted and stored at −20°C for up to one month. Before use, 4-OHT was redissolved in ethanol by shaking at 37°C for 15 minutes, diluted in 1X PBS (pH 7.4) to give a final concentration of 10 mg/ml 4-OHT, then the ethanol was evaporated by vacuum under centrifugation. The final 10 mg/ml 4-OHT solutions were always used on the day they were prepared and kept at 37°C until injection. Hippocampal 4-OHT injections were conducted using a 28-gauge needle, extending 1.0 mm beyond the tip of the guide cannulas, and connected via a polyethylene tubing (PE50) to a 1 μl Hamilton (Reno, NV) syringe controlled by an infusion pump (Harvard Apparatus. Holliston, MA). 0.3 μl of 4-OHT were delivered per brain hemisphere at a rate of 0.1 μl/minute once a day during three consecutive days. The injection needle was left in place for 2 minutes after injection to allow complete diffusion of the solution. Mice were euthanized at the end of the behavioral experiments and the dHC and the primary somatosensory cortex (S1) were collected to assess levels of *Igf2* expression.

Virus and compound 21 (C21) injections in mice—Mice were anesthetized with isoflurane mixed with oxygen, and. their skull was exposed, and holes were drilled in the skull bilaterally above the dHC. A Hamilton syringe with a 33-gauge needle mounted onto a nanopump (KD Scientific, Holliston, MA) was stereotactically inserted into the dHC (dHC, −1.7 mm posterior to bregma, ± 1.5 mm lateral from midline, −2.3 mm ventral from the skull surface). Adeno associated virus (AAV)8-hSyn-hM4Di-mCherry or AAV8-hSyn-mCherry (2.3×10^{13} genomic copies/ml, 1 μl per side; Addgene), lentivirus (LV)-Col1a1-Cre-EGFP or LV-Col1a1-EGFP ($>10^{9}$ TU/ml, 1 μl per side; constructed and packaged by VectorBuilder), AAV8-hSyn-Cre-EGFP or AAV8-hSyn-EGFP ($> 10^{13}$ genomic copies/ml, 1 μl per side; Addgene), were microinjected at a rate of 0.2 μl/min. The needle was left in place an additional 6 min following microinjection to ensure complete diffusion of the AAV and then slowly retracted. The scalp was sutured. After recovery from the surgery, mice were returned to the homecage for 2 weeks prior to experimental manipulations. C21 (HelloBio, cat# HB6124) was dissolved in PBS pH 7.4 and 0.5 mg/kg injected intraperitoneally, 30 min prior to experimental manipulations. This dosage of C21 is known to activate both DREADDs (hM4di/hM3dq) receptors and not cause any off-target effects[19]. After behavioral experiments, the mice were euthanized, and proceeded for Fluorescence-activated cell sorting (FACS) as described below.

Contextual Fear Conditioning (CFC) and immediate-shock (IS) paradigm in mice—The conditioning chamber consisted of a rectangular Perspex box (30.5 x 24.1 x 21.0 cm) with a metal grid floor (Model ENV-008 Med Associates, St Albans, Vermont, USA) through which foot shocks were delivered via a constant current scrambler circuit. CFC was carried out as described[35]. An unsignalled 2-second (s) 0.7 mA foot shock was delivered after 2 minutes in the chamber, after which the mouse remained for one more

Author Manuscript Author Manuscript Author Manuscript Author Manuscript

minute before being returned to the home cage. Animals were tested 1 day and 7 days after training. During testing, animals were placed back in the conditioning chamber for a total of 3 minutes before being returned to the home cage. No shock was delivered during the testing session. Freezing, defined as lack of movement besides heartbeat and respiration, was recorded every tenth second by a trained experimenter blind to the experimental conditions. The percentage of time spent frozen across the total number of observations was calculated[66]. The IS paradigm was used to control for non-associative memory effects of the CFC training paradigm and consisted of placing the mice in the CFC box and immediately delivering a footshock of the same intensity as that used in training. The mice were then returned to their homecage. This IS experience does not evoke CFC memory[18].

Novel object location (nOL) in mice—One and two days before training, mice were subjected to habituation sessions, each lasting 5 minutes, in an open arena (21 × 21 × 15 cm) free of bedding, lit at 110-130 lux (the first habituation session was used for open field analysis, see below for details). The walls of the arena were covered, each wall having a different color and/or high contrast pattern. For training, mice were placed into the arena with two identical objects (Mega Bloks, Quebec, Canada), freely exploring for 5 minutes. For testing (5 minutes or 4 hours later), one object remained in a constant location while the other object was moved to a new location. Mice were returned to the arena and freely explored for 5 minutes. Memory was measured as the percentage of time spent interacting with the object in the new location over the 5-minutes session. Animal behavior was video-recorded and analyzed off-line by an experimenter blind to the genotypes and drug treatments.

Open field in mice—Mice were allowed to freely explore an open field arena (21 × 21 × 15 cm) for 5 minutes, and their movements were automatically tracked using EthoVision-XT software. Locomotion was assessed using measures of total distance travelled (in cm), and average velocity (in cm/s). The arena was divided into 16 quadrants, and the time spent (s) in the four center quadrants were taken as time spent in the center, which is used as a measure of anxiety[67].

RNAscope *in situ* hybridization

Tissue Processing: Rats were euthanized, and their brains were rapidly dissected and flash frozen in isopropanol pre-cooled on dry ice. Twenty μm cryosections were mounted onto SuperFrost® Plus slides. Slides were stored at −80°C until processing for RNAscope hybridization.

RNAscope Probes: We used probes against rat insulin-like growth factor 2 (*Igf2*), and mRNA probes specific for excitatory neurons (Calcium/calmodulin-dependent protein kinase II alpha, *Camk2a*)[68], inhibitory neurons (Glutamate decarboxylase 1, *Gad1*)[69], astrocytes (10-formyltetrahydrofolate dehydrogenase, *Aldh1l1*)[70], endothelial or vascular cells (Platelet endothelial cell adhesion molecule, *Pecam1*)[71]. A highly conserved enzyme involved in regulating protein folding and maturation (Peptidylprolyl Isomerase B, *Ppib*)[72] and a bacterial enzyme involved in lysine synthesis (dihydrodipicolinate reductase, *dapB*)[73] were used as positive and negative controls, respectively. Details of the probes (i.e., NCBI

Author Manuscript Author Manuscript Author Manuscript Author Manuscript

Reference Sequence, segment of sequence targeted by probes, catalog number) can be found in Table S2. For a given tissue section, probes against *Igf2* and two cell-type markers were used, to allow for the identification of the cells expressing *Igf2*.

RNAscope hybridization: Tissue sections were processed as per manufacturer's instructions (ACD). Brain sections were removed from −80°C and were immediately immersed in 4% paraformaldehyde in 1x PBS pH 7.4 for 15 minutes at 4°C for fixation. Slides were washed three times, 5 minutes each, with 1x PBS pH 7.4, to remove the fixative solution, and then immersed in 50%, 70%, and 100% ethanol for 5 minutes each to dehydrate the tissue. Sections were air dried at room temperature, and a hydrophobic barrier was drawn with the Immedge™ hydrophobic barrier pen. Sections were pre-treated with Pretreatment 4 solution (ACD, 320513) for 30 minutes at room temperature. Sections were washed twice with 1x PBS pH 7.4. Target probes were applied to the brain sections and incubated at 40°C for 2 hours in a humid chamber. Following probe hybridization, amplification and detection steps were performed using the RNAscope® 2.5 Fluorescent Multiplex Kit for Fresh Frozen Tissue (ACD, 320293). Following the last amplification and wash step, slides were cover-slipped with ProLong™ Diamond Antifade Mountant with DAPI (Life Technologies, P36962).

RNAscope and Immunohistochemistry: After the last amplification and wash step, slides were washed with 1x PBS pH 7.4, and incubated with blocking solution comprising of 10% donkey serum and 0.1% Triton X-100 in 1x PBS pH 7.4 for 1 hour at room temperature. Slides were incubated overnight with anti-PDGFRB (R&D Systems, AF1042; 1:100) diluted in blocking buffer. Slides were washed three times, 5 minutes each, with 1x PBS pH 7.4, and incubated with donkey anti-goat 647 (Invitrogen, A21447; 1:800) and Dylight 594 labeled *Lycopersicon esculentum* (Tomato) lectin (Vector Laboratories, DL-1177; 1:300) diluted in 1x PBS pH 7.4 with 0.1% Triton X-100 for 2 hours at room temperature. Slides were then washed three times, 10 minutes each, with 1x PBS with 0.1% Triton X-100, and cover-slipped using ProLong™ Diamond Antifade Mountant with DAPI (Life Technologies, P36962).

Image Analysis: Images were acquired on a Leica Microsystems inverted TCS SP8 X confocal microscope as z-stacks at 63x magnification (glycerol immersion, HC PL APO 63×/1.30 objective) with 0.3 μm steps, 8-bit image depth. All microscope and camera settings (i.e., laser power, gain, offset, etc.) were kept constant for all images. Images were analyzed in ImageJ software using a custom macro. Maximal projection images were prepared from the z-stacks. Using the Region of Interest (ROI) Manager, cells expressing *Igf2* were manually identified and classified based on whether one of the cell-type mRNA markers was also present. Puncta of different probes appearing in the area of DAPI-stained nuclei in the same z-stack plane were considered to belong to the same cell. After ROIs were identified and classified, images were split into individual channels. The channel showing *Igf2* puncta had a threshold set such that puncta were highlighted, while minimizing background signal. The same threshold was used across all images in all experiments. After applying the threshold settings, the "Analyze particle" function was used (pixel size: 0-∞, circularity: 0-1.0), on the whole image and on each of the ROIs identified previously.

Author Manuscript Author Manuscript Author Manuscript Author Manuscript

Puncta counts and total puncta area (i.e., total number of pixels comprising the puncta) were obtained. The channel containing DAPI signal underwent contrast enhancement to 0.1% saturated pixels, Gaussian blur, and background subtraction. A binary mask was created, and the “Fill Holes” and “Watershed” functions were run sequentially to delineate individual nuclei. The “Analyze particle” function was used (pixel size: 100-1000000, circularity: 0-1.0) on the whole image and on each of the ROIs identified previously. In areas of high cell density, such as the dentate gyrus, the Watershed and Analyze particles functions were not sufficient to fully delineate individual cells. To estimate total cell numbers, the total DAPI area was divided by the average area per cell (calculated from cells that were clearly delineated). All images were analyzed by an investigator blinded to behavioral conditions.

Fluorescence-activated cell sorting (FACS) of hippocampal cells in mice— Mice were euthanized by cervical dislocation. The dorsal hippocampi were rapidly dissected on wet ice in 2% fetal bovine serum in 1x PBS pH 7.4. The choroid plexus membrane was carefully removed before preparing the tissue for FACS purification as previously described by Bowyer et al., 2012[74]. For total dorsal hippocampal samples, tissue was snap frozen on dry ice and stored at −80°C until processing for RNA extraction. For FACS of pericytes and endothelial cells, dHC from 4-5 mice were pooled together per sample, labeled with cell-specific surface markers (CD13 or CD31), and processed without permeabilization, as described by Crouch and Doetsch (2018)[13]. For sorting $COL1A1^+$ and $NeuN^+$ cells, dHC from 2-3 mice were pooled to generate sample, permeabilized using a Ebioscience™ Intracellular Fixation & Permeabilization Buffer Set (Thermo Scientific, 88-8824-00) according to the manufacturer’s instructions, and labeled with rabbit anti-Collagen1 antibody (Thermo Fisher Scientific, 600-402-103) or mouse anti-NeuN antibody (Millipore Sigma, MAB377). FACS was conducted at the Genomics Core facility at the Center for Genomics and Systems Biology at New York University. Gating strategies for pericytes and endothelial cells were set as described by Crouch and Doetsch (2018)[13] and gating strategies for neuronal cells were set as described by Guez-Barber et al., (2012)[75]. $CD13^+$, $CD31^+$, $COL1Al^+$ and $NeuN^+$ cells were collected in 1x PBS pH 7.4.

RNA extraction, reverse transcription, and real time quantitative PCR (qPCR) from mouse hippocampal tissue and FACS-purified cells—Mice were euthanized by cervical dislocation. Their brains were quickly extracted; dorsal hippocampi were rapidly dissected on wet ice in cortical dissection buffer (in mM: 2.6 KCl, 1.23 sodium phosphate monobasic, 26 sodium bicarbonate, 5 kynurenic acid, 212 sucrose, 10 dextrose, 0.5 $CaCl_2$, and 1 $MgCl_2$) and snap frozen on dry ice and stored at −80°C until ready for total hippocampal RNA extraction. Hippocampal total RNA was extracted using the RNeasy Universal Plus Mini Kit (Qiagen, 73404), and FACS-purified cell fractions were processed using the RNeasy Micro kit (Qiagen, 74004), following manufacturer’s protocol. Eluted total RNA (500 ng from total dHC, up to 50 ng from FACS-purified cell fractions) was reverse-transcribed using the QuantiTect Reverse Transcription Kit (Qiagen, 205311), according to the manufacturer’s protocol. PCR amplification consisted of: initial denaturation at 95°C for 5 minutes, followed by 40 cycles of 94°C for 30 seconds, 60°C for 30 seconds, 72°C for 20 seconds, and a final extension step at 72°C for 10 minutes. Quantitative real-time PCR analysis was done using CFX96 Touch Real-Time PCR

Author Manuscript Author Manuscript Author Manuscript Author Manuscript

Detection System (Bio-Rad, Hercules, CA, USA) with iQ SYBR Green Supermix (Bio-Rad, 107-8882). Three technical replicates were run for each sample, and the average cycle threshold (Ct) value was used for quantification using the relative quantification method. Ct values for genes of interest were normalized against the corresponding values for beta actin *(Actb)*. Glyceraldehyde-3-phosphate dehydrogenase (*Gapdh*) was used as additional loading control. Values for each sample were expressed as fold change over the average Ct value for the total dHC extract (dHC total). Primer sequences used for qPCR were described previously for *Actb, Abcc9, Slc2a1* and *Pdgfrb* in Crouch et al., 2015[13], *Igf2* in Schmeisser et al., 2012[60] and Abraham et al., 2011[76], *Col1a1* in Sokolov et al., 1995[77], *NeuN* in Wang et al., (2015)[78], and *Gapdh* in Pandey et al., 2020[79]. Primer sequences are listed in Table S3.

Igf2-tdTomato-H2B immunostaining and cell type-specific protein colocalization analyses—For tdTomato immunostaining and cell type-specific protein colocalization analyses following CFC and untrained conditions CFC was conducted at CSH laboratories in a rectangular Perspex box (18 cm × 18 cm × 30 cm) with a metal grid floor connected to a H13–15 shock generator (Coulbourn Instruments) through which foot shocks were delivered via a constant current scrambler circuit. CFC protocol was carried out as described under the section Contextual Fear Conditioning (CFC) in mice. One day after training, mice were deeply anesthetized by *i.p.* injections of a ketamine (60 mg/kg) and medetomidine (0.5 mg/kg) cocktail and transcardially perfused with 15 ml cold saline (0.9% NaCl) followed by 30 ml cold neutral buffered formaldehyde (4% w/v in phosphate buffer, pH 7.4). The brains were dissected and processed for serial two-photon tomography (STPT), as described previously[80].

Serial two-photon tomography (STPT): Briefly, brains were embedded in 4% agarose in 0.05M PB, cross-linked in 0.2% sodium borohydride solution (in 0.05 M sodium borate buffer, pH 9.0-9.5). The entire brain (including the olfactory bulb and the cerebellum) was imaged with a high-speed 2-photon microscope with integrated vibratome (at CSHL) at 1μm-1μm x-y resolution for a depth of 50 μm on a TissueCyte 1000 (TissueVision). The 2-photon excitation wavelength was 910 nm, which efficiently excites tdTom fluorophore. A 560 nm dichroic mirror (Chroma, T560LPXR) and bandpass filters (Semrock FF01-520/35 an) were used to separate green and red fluorescent signals. After STPT was complete, coronal slices were prepared using a vibrating blade microtome (Leica Biosystems VT1000S, at CSHL). Brain sections were collected and stored in cryoprotectant at −20C for immunohistochemical analysis.

Immunohistochemical double staining: Sections were washed with 1x PBS pH 7.4 three times for 10 minutes each, and then incubated with blocking buffer consisting of 10% normal donkey serum and 0.6% Triton X-100 in 1x PBS pH 7.4 for 2 hours at room temperature. Primary antibodies (goat anti-PDGFRB antibody, R&D Systems, AF1042, 1:100; rat anti-CD31, BD Pharmingen, 557355, 2.5 μg/ml; rabbit anti-Collagen1 antibody, Thermo Fisher Scientific, 600-402-103, 1:500; rabbit anti-IBA1 antibody, Fujifilm Wako Chemicals, Cat. 019-19741, 1:1000) were diluted in blocking buffer and incubated for 48 hours at 4C. Sections were washed with wash buffer (0.4% Triton in 1x PBS pH 7.4) three times, 10 minutes each wash, and incubated with secondary antibodies (Donkey-anti

Author Manuscript Author Manuscript Author Manuscript Author Manuscript

rat-488, Invitrogen, A21208; Donkey-anti-goat-647, Invitrogen, A21447; goat-anti-rabbit Alexa Fluor 488, Invitrogen, A11034; goat-anti-rabbit Alexa Fluor 568, Invitrogen, A11036) at a dilution of 1:800 in blocking buffer for 2 hours at room temperature. Sections were washed with wash buffer three times for 10 minutes each, followed by two washes, 5 minutes each, with 1x PBS pH 7.4. Sections were counterstained with DAPI (Thermo Scientific, 62247; 1:1,000) diluted in 1x PBS pH 7.4 for 10 minutes, then washed with 1x PBS pH 7.4, three times for 1 minute each. Sections were mounted onto SuperFrost® Plus slides and coverslipped with ProLong™ Diamond Antifade Mountant (Invitrogen, P36961).

Confocal Microscopy and Analysis: Images were acquired on a Leica Microsystems TCS SP8 X or Zeiss LSM 710 (at CSHL) confocal microscope as z-stacks at 40x or 20x magnification with 2 μm steps, 8-bit image depth. All microscope and camera settings (i.e., laser power, gain, offset, etc.) were identical for all images within an experiment. Images were analyzed in ImageJ software using a custom macro. Maximal projection images were created from the z-stacks and converted into 8-bit grayscale images. These projection images were thresholded to capture tdTomato-labeled nuclei while minimizing background; the same threshold parameters were used for all images. The “Analyze particle” function was used to identify and individual tdTomato-labeled nuclei as ROIs. These ROIs were applied to the original image, and the fluorescent intensity and area of the tdTomato signal within each ROI was measured. The “Analyze particle” function was also used to measure the total DAPI-labeled area. The total number of tdTomato cells were normalized to the total DAPI-labeled nuclei in each image.

Data Analyses of tdTomato and IBA1 or COL1A1 co-staining: Images were acquired on a Leica Microsystems TCS SP8 confocal microscope as z-stacks at 63x or 40x magnification with 1 μm steps, 8-bit image depth. All microscope and camera settings (i.e., laser power, gain, offset, etc.) were identical for all images within an experiment. No adjustments for brightness or contrast were made, and images were exported as TIFF-files. Colocalization analyses was performed using ImageJ. To quantify the colocalization, we used a method previously described by Wallrafen et al., 2018[81]. Briefly, the background was subtracted from the 8-bit grey images using the rolling ball radius: 100 pixels for both red (tdTomato) and green (IBA1 or COL1A1) channels. The number of tdTomato+, IBA1+, COL1A1+, tdTomato+/IBA1+ and tdTomato+/Col1a1+ cells were normalized to the total DAPI count. For tdTomato+/IBA1+ colocalization analyses, the data were expressed as % of tdTomato+ cells in untrained mice.

Hippocampal dissection and western blot analysis—Mice were euthanized by decapitation. Their dorsal hippocampi were collected from bregma −2.8 mm to −5.4 mm using a brain matrix. The collected tissues were snap-frozen on dry ice. Protein extraction followed by western blot analyses were carried out as described previously[1]. The tissues were homogenized in radioimmunoprecipitation assay (RIPA) buffer (150 mM NaCl, 1% Triton X-100, 0.5% sodium deoxycholate, 0.1% SDS, 5 mM EDTA, 10% glycerol, 50 mM Tris, pH 8.0) supplemented with 0.5 mM PMSF, 2 mM DTT, 1 mM EGTA, 1 μM microcystin LR, 10 mM NaF, 1 mM NaOV, benzamidine, protease inhibitor cocktail and phosphatase inhibitor cocktail II and III (used as recommended

Author Manuscript Author Manuscript Author Manuscript Author Manuscript

by the manufacturer; Sigma, St. Louis, MO). Protein concentrations were determined by the Bio-Rad protein assay (Bio-Rad Laboratories, Hercules, CA). Twenty micrograms of total protein extract per lane was resolved in 4-20% gradient gel (Bio-Rad Laboratories, Hercules, CA) and transferred to 0.2 μm Immobilon-FL membranes (Millipore, Billerica, MA). After blocking in Li-COR Blocking buffer (Li-COR, Lincoln, NE), membranes were incubated with primary antibodies: rabbit anti-IGF2 (1:500, Abcam, ab9574); rabbit antication-independent mannose 6 phosphate receptor (1:10,000, Abcam, ab124767); rabbit anti-Arc (1:2,000, Synaptic Systems, 156003); rabbit anti-c-Fos (1:2,000, Cell Signaling Technology, 2250); rabbit anti-EGR1 (1:1,000, Cell Signaling Technology, 4153); anti-actin (1:20,000, Santa Cruz Biotechnology, sc-47778). The latter was used for loading normalization. Secondary antibodies: anti-rabbit IRDye800CW and anti-mouse IRDye680 (1:20,000, Li-COR, Lincoln, NE). Membranes were scanned on the Li-COR Odyssey imager under non-saturating conditions. Data were quantified using pixel intensities with the Odyssey software according to manufacturer protocols (Li-COR, Lincoln, NE).

Immediate early gene (IEG) immunofluorescence staining—Immunofluorescent staining, confocal imaging, and analyses of IEGs (ARC, FOS and EGR1) and were done as previously described[79]. Briefly, mice were anesthetized with an *i.p.* injection of 750 mg/kg chloral hydrate and transcardially perfused with 4% paraformaldehyde (Sigma, 158127) in 1x phosphate-buffered saline (PBS; 137 mM NaCl [Sigma, S3014], 2.7 mM KCl [Sigma, P9541], 10 mM Na2HPO4 [Sigma, S5136] and 1.8 mM KH2PO4 [Sigma, P5655], pH 7.4). Their brains were postfixed in the same solution overnight at 4°C, followed by 30% sucrose (30 g sucrose [Sigma, S0389] in 100 ml of 1x PBS, pH 7.4) for 72 hours. 20 μm brain sections were immunostained using free-floating incubations. Immunostaining was performed with antigen retrieval, which consisted of boiling the brain sections in nanopure H2O for 2 min. The sections were then incubated with the blocking solution (1x PBS, pH 7.4 with 0.25% Triton X-100 [Sigma, T8787], 4% normal goat serum [Cell Signaling Technology, 5425], 1% bovine serum albumin [Sigma, A2058]) for 2 hours at room temperature, followed by incubation with the primary antibodies in the blocking solution for 24 hours at 4°C. The following primary antibodies were used: rabbit anti-ARC (1:2,000, Synaptic Systems, 156003); rabbit anti-FOS (1:2,000, Cell Signaling Technology, 2250); rabbit anti-EGR1 (1:1,000, Cell Signaling Technology, 4153). Subsequently the brain sections were washed 3 times with 1x PBST (1x PBS, pH 7.4 containing 0.025% Triton X-100), and then incubated with the secondary antibody, which consisted of goat-anti-rabbit Alexa Fluor 488 (Invitrogen, A11034), goat-anti-rabbit Alexa Fluor 568 (Invitrogen, A11036) or goat anti-rabbit Alexa Fluor 647 (Invitrogen, A21244) at 1:1000 dilution in 1x PBS pH 7.4 for 2 hours at room temperature. The sections were washed 3 times with 1x PBST, rinsed with 1x PBS, pH 7.4, and then mounted with Prolong Diamond antifade mountant with DAPI (Invitrogen, P36962).

Two sections between bregma −3.6 mm and −4.2 mm were used for each set of staining. Four images per subregion (CA1 and DG) per side for each animal were captured as z-stacks at 63x magnification with 1 μm steps, 8-bit image depth using a Leica TCS SP8 confocal microscope (Leica microsystems, Wetzlar, Germany). In all immunochemistry experiments n = 4 mice per group were used. For each mouse, 16 images (8 per side) were quantified

Author Manuscript Author Manuscript Author Manuscript Author Manuscript

and averaged. Experimenters blinded to experimental conditions quantified the images using ImageJ software (US, National Institutes of Health) and automated custom macro programs. For intensity measurements, images were processed to remove background and outlier noise. All images in each experiment were processed using the same parameters. The z-stack image was processed to generate the maximum projection image and the intensity was measured using ImageJ plugin. Quantifications of markers in the cellular and molecular layers of CA1 and DG areas were conducted by using a modification of a previously described method that measured immunofluorescence in hippocampal cell soma and processes[79]. Quantifications of immunofluorescence intensity were performed on 63x 8-bit grayscale images and images were acquired using the same parameters every time. Using the free-hand line tool, we delimited the perinuclear areas visualized with the DAPI channel in the CA1 *stratum pyramidale* (40 μm length) and DG *stratum granulosum* (60 μm length) and saved them as "soma-ROI". An area outside to the soma-ROI, of 50 μm in length in the CA1 *stratum radiatum* and of 70 μm in length in the DG *stratum moleculare* were saved as "process-ROI". For each image, a rolling ball radius of 10 was uniformly applied to subtract the background from the 8-bit grayscale images; the background was established on parallel sections incubated with only the secondary antibody. The soma-ROI and process-ROI were overlaid on the IEG images, and the mean gray values of the image stacks normalized over the number DAPI counts (ImageJ plugin) in each image were taken as the mean immunofluorescence intensity values.

Analyses of PDGFRB immunostaining (pericyte coverage)—PDGFRB+ pericyte coverage were determined as previously described[82]. Tissue sections were prepared as described under the immunofluorescent staining section. Sections were incubated with goat anti-mouse PDGFRB antibody (R&D systems, AF1042) overnight at 4°C, followed by incubation with Alexa Fluor 647 conjugated donkey anti-goat IgG (Invitrogen, A21447) at a dilution of 1:1000 in 1x PBS pH 7.4, for 1 hour at room temperature. The sections were washed 3 times with 1x PBST, rinsed with 1x PBS, pH 7.4, and then mounted with Prolong Diamond antifade mountant with DAPI (Invitrogen, P36962).

All images were acquired using a Leica TCS SP8 confocal microscope (Leica microsystems, Wetzlar, Germany) at 40x magnification. In each mouse, four different 200 μm × 200 μm region of interest (ROI) were analyzed per cellular and molecular layer in each hippocampal subregion (CA1, CA3 and DG) and SLM (SLM/*stratum moleculare* layer of DG) in four non-adjacent sections. PDGFRB positive immunofluorescent signals from brain microvessels < 6 μm in diameter were individually subjected to threshold processing and the areas occupied by their respective signals were quantified using the NIH Image J software Area measurement tool. The percent of PDGFRB pericyte coverage was then determined by normalizing the PDGFRB-positive signal to the total area under ROI imaged in different subregions of the dorsal hippocampal section.

Evans blue assay for blood-brain barrier permeability—EB assay according to the method described by Radu and Chernoff, 2013[83].

Author Manuscript Author Manuscript Author Manuscript Author Manuscript

Preparation of Evans Blue dye (EB) solution: A 0.5% solution of EB dye was prepared in 1x PBS, pH 7.4 and the solution was filter-sterilized to remove any undissolved particulate matter.

Injection of EB dye into lateral tail vein of mice and tissue collection: Mice were restrained and a 200 μl of EB solution was slowly injected into the lateral tail vein towards the direction of their head. One hour following injection, the mice were euthanized through cervical dislocation. Pictures of the freshly dissected brains were taken to show differences in EB extravasation in each condition. Hippocampi from each mouse were collected in a microfuge tube and their weights were recorded. To each tissue sample tube, 500 μl formamide was added and all the tubes were incubated at 55°C on a water bath for 24 hours to extract EB from the tissue. The lipopolysaccharide (LPS) (Sigma, L6011) was dissolved in 1x PBS, pH 7.4 to a concentration of 1mg/4 ml. LPS or 1x PBS, pH 7.4 (Vehicle) were injected *i.p.* into each mouse (4 ml/kg body weight). One hour later, EB dye was injected into the tail vein of these mice.

Quantification of extravasated EB in hippocampal tissue: The Formamide/EB mixture was centrifuged at 2000g for 5 minutes to pellet any remaining tissue fragments. Absorbance at 610 nm was measured using Spectrophotometer (Genesys 10UV, Thermo Spectronic) to assay the amount of EB dye in the solution. A 500 μl formamide solution was used as blank. The EB concentration in each sample was calculated according to a standard curve prepared with a range of 100 ng/ml to 1 μg/ml of EB in 1x PBS, pH 7.4. The amount of EB dye extravasated (in ng) were normalized to the weight of hippocampal tissue (in mg).

Quantification and Statistical analysis—Data were analyzed using Prism 7 (GraphPad Software Inc.). No statistical method was used to predetermine sample sizes; sample size was determined based on our experience and the sample size used in similar studies[1]. Replications: All experiments were carried out at least with 2 cohorts of animals for internal replication. The number of replicas is indicated in the figure legends. One-way ANOVAs followed by Tukey's post-hoc analyses were performed when comparing groups for which a pairwise comparison of each group was required. Mixed-effects analyses followed by Bonferroni's multiple comparison tests or Two-way ANOVAs (ordinary or repeated measure) followed by Bonferroni's or Tukey's or Sidak's post-hoc tests were used when two factors (such as treatment and testing) were compared. When two groups were compared, Student's t-tests were used. All analyses were two-tailed. Kolmogorov-Smirnov test was used to compare the cumulative frequency distributions. The significance of the results was accepted at $p < 0.05$.

Supplementary Material

Refer to Web version on PubMed Central for supplementary material.

Acknowledgements

This work was supported by the NIH grant MH065635 to C.M.A. Work to generate the *Igf2*-floxed mice in M.C. lab was supported by Biotechnology and Biological Sciences Research Council, UK (grant BB/H003312/1) and the

Author Manuscript Author Manuscript Author Manuscript Author Manuscript

Medical Research Council, UK (grants MRC_MC_UU_00014/4 and MRC_MC_UU_12012/5); J.T. was supported by DFG Mercator Fellowship (DFG grant number TU 585/1-1).

References

1. Chen DY, Stern SA, Garcia-Osta A, Saunier-Rebori B, Pollonini G, Bambah-Mukku D, Blitzer RD, and Alberini CM (2011). A critical role for IGF-II in memory consolidation and enhancement. Nature 469, 491–497. doi: 10.1038/nature09667. [PubMed: 21270887]
2. Bergman D, Halje M, Nordin M and Engström W (2013). Insulin-like growth factor 2 in development and disease: a mini-review. Gerontology 59, 240–249. doi: 10.1159/000343995. [PubMed: 23257688]
3. Iadecola C. (2017). The neurovascular unit coming of age: a journey through neurovascular coupling in health and disease. Neuron 96, 17–42. doi: 10.1016/j.neuron.2017.07.030. [PubMed: 28957666]
4. Ross JM, Kim C, Allen D, Crouch EE, Narsinh K, Cooke DL, Abla AA, Nowakowski TJ, and Winkler EA (2020). The expanding cell diversity of the brain vasculature. Front. Physiol 11, 600767. doi: 10.3389/fphys.2020.600767. [PubMed: 33343397]
5. Uhlirova H, Kılıç K, Tian P, Thunemann M, Desjardins M, Saisan PA, Sakadžić S, Ness TV, Mateo C, Cheng Q, et al. (2016). Cell type specificity of neurovascular coupling in cerebral cortex. Elife 5, e14315. doi: 10.7554/eLife.14315. [PubMed: 27244241]
6. Wang Z, Portier BP, Gruver AM, Bui S, Wang H, Su N, Vo HT, Ma XJ, Luo Y, Budd GT, et al. (2013). Automated quantitative RNA in situ hybridization for resolution of equivocal and heterogeneous ERBB2 (HER2) status in invasive breast carcinoma. J. Mol. Diagn 15, 210–219. doi: 10.1016/j.jmoldx.2012.10.003. [PubMed: 23305906]
7. Wang F, Flanagan J, Su N, Wang LC, Bui S, Nielson A, Wu X, Vo HT, Ma XJ, and Luo Y (2012). RNAscope: a novel in situ RNA analysis platform for formalin-fixed, paraffin-embedded tissues. J. Mol. Diagn 14, 22–29. doi: 10.1016/j.jmoldx.2011.08.002. [PubMed: 22166544]
8. Ye X, Kohtz A, Pollonini G, Riccio A, and Alberini CM (2015). Insulin like growth factor 2 expression in the rat brain both in basal condition and following learning predominantly derives from the maternal allele. PLoS One 10, e0141078. doi: 10.1371/journal.pone.0141078. [PubMed: 26495851]
9. Hamilton NB, Attwell D, and Hall CN (2010). Pericyte-mediated regulation of capillary diameter: a component of neurovascular coupling in health and disease. Front. Neuroenergetics 2: 5. doi: 10.3389/fnene.2010.00005. [PubMed: 20725515]
10. Robertson RT, Levine ST, Haynes SM, Gutierrez P, Baratta JL, Tan Z, and Longmuir KJ (2015). Use of labeled tomato lectin for imaging vasculature structures. Histochem. Cell. Biol 143, 225–234. doi: 10.1007/s00418-014-1301-3. [PubMed: 25534591]
11. Winkler EA, Bell RD, and Zlokovic BV (2010). Pericyte-specific expression of PDGF beta receptor in mouse models with normal and deficient PDGF beta receptor signaling. Mol. Neurodegener 5, 32. doi: 10.1186/1750-1326-5-32. [PubMed: 20738866]
12. Kunz J, Krause D, Kremer M, and Dermietzel R (1994). The 140-kDa protein of blood-brain barrier-associated pericytes is identical to aminopeptidase N. J. Neurochem 62, 2375–2386. doi: 10.1046/j.1471-4159.1994.62062375.x. [PubMed: 7910634]
13. Crouch EE, and Doetsch F (2018). FACS isolation of endothelial cells and pericytes from mouse brain microregions. Nat. Protoc 13, 738–751. doi: 10.1038/nprot.2017.158. [PubMed: 29565899]
14. Bondjers C, He L, Takemoto M, Norlin J, Asker N, Hellström M, Lindahl P, and Betsholtz C (2006). Microarray analysis of blood microvessels from PDGF-B and PDGF-Rbeta mutant mice identifies novel markers for brain pericytes. FASEB J. 20, 1703–1705. doi: 10.1096/fj.05-4944fje. [PubMed: 16807374]
15. Daneman R, Zhou L, Agalliu D, Cahoy JD, Kaushal A, and Barres BA (2010). The mouse blood-brain barrier transcriptome: a new resource for understanding the development and function of brain endothelial cells. PLoS One 5, e13741. doi: 10.1371/journal.pone.0013741. [PubMed: 21060791]
16. Vanlandewijck M, He L, Mäe MA, Andrae J, Ando K, Del Gaudio F, Nahar K, Lebouvier T, Laviña B, Gouveia L, et al. (2018). A molecular atlas of cell types and zonation in the brain vasculature. Nature 554, 475–480. doi: 10.1038/nature25739. [PubMed: 29443965]

Author Manuscript Author Manuscript Author Manuscript Author Manuscript

17. Bonney SK, Sullivan LT, Cherry TJ, Daneman R, and Shih AYJ (2021). Distinct features of brain perivascular fibroblasts and mural cells revealed by in vivo two-photon imaging. Cereb. Blood Flow Metab. 271678X211068528. doi: 10.1177/0271678X211068528.

18. Fanselow MS (1986). Associative vs topographical accounts of the immediate shock-freezing deficit in rats: Implication for the response selection rules governing species-specific defensive reactions. Learn. Motiv 17, 16–39. doi: 10.1016/0023-9690(86)90018-4.

19. Thompson KJ, Khajehali E, Bradley SJ, Navarrete JS, Huang XP, Slocum S, Jin J, Liu J, Xiong Y, Olsen RHJ, et al. (2018). DREADD Agonist 21 Is an Effective Agonist for Muscarinic-Based DREADDs in Vitro and in Vivo. ACS Pharmacol Transl Sci. 1, 61–72. doi: 10.1021/acsptsci.8b00012. [PubMed: 30868140]

20. Armulik A, Genove G, and Betsholtz C (2011). Pericytes: developmental, physiological, and pathological perspectives, problems, and promises. Dev. Cell 21, 193–215. doi: 10.1016/j.devcel.2011.07.001. [PubMed: 21839917]

21. Sweeney MD, Ayyadurai S, and Zlokovic BV (2016). Pericytes of the neurovascular unit: key functions and signaling pathways. Nat. Neurosci 19, 771–783. doi: 10.1038/nn.4288. [PubMed: 27227366]

22. Daneman R, and Prat A (2015). The blood-brain barrier. Cold Spring Harb Perspect Biol. 7, a020412. doi: 10.1101/cshperspect.a020412. [PubMed: 25561720]

23. Hall CN, Reynell C, Gesslein B, Hamilton NB, Mishra A, Sutherland BA, O'Farrell FM, Buchan AM, Lauritzen M, and Attwell D (2014). Capillary pericytes regulate cerebral blood flow in health and disease. Nature 508, 55–60. doi: 10.1038/nature13165. [PubMed: 24670647]

24. Sweeney MD, Zhao Z, Montagne A, Nelson AR, and Zlokovic BV (2019). Blood-brain barrier: from physiology to disease and back. Physiol. Rev 99, 21–78. doi: 10.1152/physrev.00050.2017. [PubMed: 30280653]

25. Nortley R, Korte N, Izquierdo P, Hirunpattarasilp C, Mishra A, Jaunmuktane Z, Kyrargyri V, Pfeiffer T, Khennouf L, Madry C, et al. (2019). Amyloid beta oligomers constrict human capillaries in Alzheimer's disease via signaling to pericytes. Science 365, eaav9518. doi: 10.1126/science.aav9518. [PubMed: 31221773]

26. Attwell D, Mishra A, Hall CN, O'Farrell FM, and Dalkara T (2016). What is a pericyte? J. Cereb. Blood Flow. Metab 36, 451–455. doi: 10.1177/0271678X15610340. [PubMed: 26661200]

27. Ito D, Imai Y, Ohsawa K, Nakajima K, Fukuuchi Y, and Kohsaka S (1998). Microglia-specific localisation of a novel calcium binding protein, Iba1. Molecular brain research 57, 1–9. doi: 10.1016/s0169-328x(98)00040-0. [PubMed: 9630473]

28. Haley VL, Barnes DJ, Sandovici I, Constancia M, Graham CF, Pezzella F, Bühnemann C, Carter EJ, Hassan AB (2012). Igf2 pathway dependency of the Trp53 developmental and tumour phenotypes. EMBO Molecular Medicine 4, 705–718. doi: 10.1002/emmm.201101105. [PubMed: 22674894]

29. Hammerle CM, Sandovici I, Brierley GV, Smith NM, Zimmer WE, Zvetkova I, Prosser HM, Sekita Y, Lam BYH, Ma M, et al. (2020). Mesenchyme-derived IGF2 is a major paracrine regulator of pancreatic growth and function. PLoS Genet. 16, e1009069. doi: 10.1371/journal.pgen.1009069. [PubMed: 33057429]

30. Cuervo H, Pereira B, Nadeem T, Lin M, Lee F, Kitajewski J, and Lin CS (2017). PDGFRbeta-P2A-CreER(T2) mice: a genetic tool to target pericytes in angiogenesis. Angiogenesis 20, 655–662. doi: 10.1007/s10456-017-9570-9. [PubMed: 28752390]

31. Ennaceur A. (2010). One-trial object recognition in rats and mice: Methodological and theoretical issues. Behav. Brain Res 215, 244–254. doi: 10.1016/j.bbr.2009.12.036. [PubMed: 20060020]

32. Kim JJ, and Fanselow MS (1992). Modality-specific retrograde amnesia of fear. Science 256, 675–677. doi: 10.1126/science.1585183. [PubMed: 1585183]

33. Kraeuter AK, Guest PC, and Sarnyai Z (2019). The open field test for measuring locomotor activity and anxiety-like behavior. Methods Mol. Biol 19, 99–103. doi: 10.1007/978-1-4939-8994-2_9.

34. Gallo FT, Katche C, Morici JF, Medina JH, and Weisstaub NV (2018). Immediate early genes, memory and psychiatric disorders: Focus on c-Fos, Egr1 and Arc. Front. Behav. Neurosci 12, 79. doi: 10.3389/fnbeh.2018.00079. [PubMed: 29755331]

Author Manuscript Author Manuscript Author Manuscript Author Manuscript

35. Yu XW, Pandey K, Katzman AC, and Alberini CM (2020). A role for CIM6P/IGF2 receptor in memory consolidation and enhancement. Elife 9, e54781. doi: 10.7554/eLife.54781. [PubMed: 32369018]
36. Stylianopoulou F, Herbert J, Soares MB, and Efstratiadis A (1988). Expression of the insulin-like growth factor II gene in the choroid plexus and the leptomeninges of the adult rat central nervous system. Proc. Natl. Acad. Sci. U S A 85, 141–145. doi: 10.1073/pnas.85.1.141. [PubMed: 3422410]
37. Logan A, Gonzalez AM, Hill DJ, Berry M, Gregson NA, and Baird A (1994). Coordinated pattern of expression and localization of insulin-like growth factor-II (IGF-II) and IGF-binding protein-2 in the adult rat brain. Endocrinology 135, 2255–2264. doi: 10.1210/endo.135.5.7525264. [PubMed: 7525264]
38. Ferrón SR, Radford EJ, Domingo-Muelas A, Kleine I, Ramme A, Gray D, Sandovici I, Constancia M, Ward A, Menheniott TR, et al. (2015). Differential genomic imprinting regulates paracrine and autocrine roles of IGF2 in mouse adult neurogenesis. Nat. Commun 6, 8265. doi: 10.1038/ncomms9265. [PubMed: 26369386]
39. Kalish BT, Cheadle L, Hrvatin S, Nagy MA, Rivera S, Crow M, Gillis J, Kirchner R, and Greenberg ME (2018). Single-cell transcriptomics of the developing lateral geniculate nucleus reveals insights into circuit assembly and refinement. Proc. Natl. Acad. Sci. U S A 115, E1051–E1060. doi: 10.1073/pnas.1717871115. [PubMed: 29343640]
40. Sheikh BN, Bondareva O, Guhathakurta S, Tsang TH, Sikora K, Aizarani N, Sagar, Holz H, Grün D, Hein L, et al. (2019). Systematic identification of cell-cell communication networks in the developing brain. iScience 21, 273–287. doi: 10.1016/j.isci.2019.10.026. [PubMed: 31677479]
41. Molnár K, Mészáros Á, Fazakas C, Kozma M, Győri F, Reisz Z, Tiszlavicz L, Farkas AE, Nyúl-Tóth Á, Haskó J, et al. (2020). Pericyte-secreted IGF2 promotes breast cancer brain metastasis formation. Mol. Oncol 14, 2040–2057. doi: 10.1002/1878-0261.12752. [PubMed: 32534480]
42. Moser EI, Kropff E, and Moser MB (2008). Place cells, grid cells, and the brain's spatial representation system. Annu. Rev. Neurosci 31, 69–89. doi: 10.1146/annurev.neuro.31.061307.090723. [PubMed: 18284371]
43. Braak H, Braak E, and Bohl J (1993). Staging of Alzheimer-related cortical destruction. Eur. Neurol 33, 403–408. doi: 10.1159/000116984. [PubMed: 8307060]
44. Mellott TJ, Pender SM, Burke RM, Langley EA, and Blusztajn JK (2014). IGF2 ameliorates amyloidosis, increases cholinergic marker expression and raises BMP9 and neurotrophin levels in the hippocampus of the APPswePS1dE9 Alzheimer's disease model mice. PLoS One 9, e94287. doi: 10.1371/journal.pone.0094287. [PubMed: 24732467]
45. Pascual-Lucas M, Viana da Silva S, Di Scala M, Garcia-Barroso C, González-Aseguinolaza G, Mulle C, Alberini CM, Cuadrado-Tejedor M, and Garcia-Osta A (2014). Insulin-like growth factor 2 reverses memory and synaptic deficits in APP transgenic mice. EMBO Mol. Med 6, 1246–1262. doi: 10.15252/emmm.201404228. [PubMed: 25100745]
46. Steinmetz AB, Johnson SA, Iannitelli DE, Pollonini G, and Alberini CM (2016). Insulin-like growth factor 2 rescues aging-related memory loss in rats. Neurobiol. Aging 44, 9–21. doi: 10.1016/j.neurobiolaging.2016.04.006. [PubMed: 27318130]
47. Montagne A, Barnes SR, Sweeney MD, Halliday MR, Sagare AP, Zhao Z, Toga AW, Jacobs RE, Liu CY, Amezcua L, et al. (2015). Blood-brain barrier breakdown in the aging human hippocampus. Neuron 85, 296–302. doi: 10.1016/j.neuron.2014.12.032. [PubMed: 25611508]
48. Witter MP, Griffioen AW, Jorritsma-Byham B, and Krijnen JL (1988). Entorhinal projections to the hippocampal CA1 region in the rat: an underestimated pathway. Neurosci. Lett 85, 193–198. doi: 10.1016/0304-3940(88)90350-3. [PubMed: 3374835]
49. Wouterlood FG, Saldana E, and Witter MP (1990). Projection from the nucleus reuniens thalami to the hippocampal region: light and electron microscopic tracing study in the rat with the anterograde tracer Phaseolus vulgaris-leucoagglutinin. J. Comp. Neurol 296, 179–203. doi: 10.1002/cne.902960202. [PubMed: 2358531]
50. Pikkarainen M, Ronkko S, Savander V, Insausti R, and Pitkanen A (1999). Projections from the lateral, basal, and accessory basal nuclei of the amygdala to the hippocampal formation in rat. J. Comp. Neurol 403, 229–260. [PubMed: 9886046]

Author Manuscript Author Manuscript Author Manuscript Author Manuscript

51. Iwai E, and Yukie M (1988). A direct projection from hippocampal field CA1 to ventral area TE of inferotemporal cortex in the monkey. Brain Res. 444, 397–401. doi: 10.1016/0006-8993(88)90955-9. [PubMed: 2834025]
52. Hartmann DA, Underly RG, Grant RI, Watson AN, Lindner V, and Shih AY (2015). Pericyte structure and distribution in the cerebral cortex revealed by high-resolution imaging of transgenic mice. Neurophotonics 2, 041402. doi: 10.1117/1.NPh.2.4.041402. [PubMed: 26158016]
53. Grant RI, Hartmann DA, Underly RG, Berthiaume AA, Bhat NR, and Shih AY (2019). Organizational hierarchy and structural diversity of microvascular pericytes in adult mouse cortex. J. Cereb. Blood Flow Metab 39, 411–425. doi: 10.1177/0271678X17732229. [PubMed: 28933255]
54. Sandovici I, Hammerle CM, Virtue S, Vivas-Garcia Y, Izquierdo-Lahuerta A, Ozanne SE, Vidal-Puig A, Medina-Gómez G, and Constância M (2021). Autocrine IGF2 programmes β-cell plasticity under conditions of increased metabolic demand. Sci. Rep 11, 7717. doi: 10.1038/s41598-021-87292-x. [PubMed: 33833312]
55. Herr F, Liang OD, Herrero J, Lang U, Preissner KT, Han VK, and Zygmunt M (2003). Possible angiogenic roles of insulin-like growth factor II and its receptors in uterine vascular adaptation to pregnancy. J Clin Endocrinol Metab 88, 4811–7-10. doi: 10.1210/jc.2003-030243. [PubMed: 14557459]
56. Lewitt MS, and Boyd GW (2019). The role of insulin-like growth factors and insulin-like growth factor-binding proteins in the nervous system. Biochem. Insights 12, 1178626419842176. doi: 10.1177/1178626419842176. [PubMed: 31024217]
57. Ishii DN (1989). Relationship of insulin-like growth factor II gene expression in muscle to synaptogenesis. Proc. Natl. Acad. Sci. U S A 86, 2898–2902. doi: 10.1073/pnas.86.8.2898. [PubMed: 2704752]
58. Agis-Balboa RC, Arcos-Diaz D, Wittnam J, Govindarajan N, Blom K, Burkhardt S, Haladyniak U, Agbemenyah HY, Zovoilis A, Salinas-Riester G, et al. (2011). A hippocampal insulin-growth factor 2 pathway regulates the extinction of fear memories. EMBO J. 30, 4071–4083. doi: 10.1038/emboj.2011.293. [PubMed: 21873981]
59. Lehtinen MK (2011). The cerebrospinal fluid provides a proliferative niche for neural progenitor cells. Neuron 69, 893–905. doi: 10.1016/j.neuron.2011.01.023. [PubMed: 21382550]
60. Schmeisser MJ, Baumann B, Johannsen S, Vindedal GF, Jensen V, Hvalby ØC, Sprengel R, Seither J, Maqbool A, Magnutzki A, et al. (2012). IkappaB kinase/nuclear factor kappaB-dependent insulin-like growth factor 2 (Igf2) expression regulates synapse formation and spine maturation via Igf2 receptor signaling. J. Neurosci 32, 5688–5703. doi: 10.1523/JNEUROSCI.0111-12.2012. [PubMed: 22514330]
61. Stern SA, Kohtz AS, Pollonini G, and Alberini CM (2014). Enhancement of memories by systemic administration of insulin-like growth factor II. Neuropsychopharmacology 39, 2179–2190. doi: 10.1038/npp.2014.69. [PubMed: 24642597]
62. Lee Y, Lee YW, Gao Q, Lee Y, Lee HE, and Ryu JH (2015). Exogenous insulin-like growth factor 2 administration enhances memory consolidation and persistence in a time-dependent manner. Brain Res. 1622, 466–473. doi: 10.1016/j.brainres.2015.07.002. [PubMed: 26168901]
63. Pardo M, Cheng Y, Velmeshev D, Magistri M, Eldar-Finkelman H, Martinez A, Faghihi MA, Jope RS, and Beurel E (2017). Intranasal siRNA administration reveals IGF2 deficiency contributes to impaired cognition in Fragile X syndrome mice. JCI insight, 2, e91782. doi: 10.1172/jci.insight.91782. [PubMed: 28352664]
64. Alberini CM, and Chen DY (2012). Memory enhancement: consolidation, reconsolidation and insulin-like growth factor 2. Trends Neurosci. 35, 274–283 doi: 10.1016/j.tins.2011.12.007. [PubMed: 22341662]
65. Nikolakopoulou AM, Montagne A, Kisler K, Dai Z, Wang Y, Huuskonen MT, Sagare AP, Lazic D, Sweeney MD, Kong P, et al. (2019). Pericyte loss leads to circulatory failure and pleiotrophin depletion causing neuron loss. Nat. Neurosci 22, 1089–1098. doi: 10.1038/s41593-019-0434-z. [PubMed: 31235908]
66. Schrick C, Fischer A, Srivastava DP, Tronson NC, Penzes P, and Radulovic J (2007). N-cadherin regulates cytoskeletally associated IQGAP1/ERK signaling and memory formation. Neuron 55, 786–798. doi: 10.1016/j.neuron.2007.07.034. [PubMed: 17785185]

Author Manuscript Author Manuscript Author Manuscript Author Manuscript

67. Bailey K,R, and Crawley JN (2009). Anxiety-Related Behaviors in Mice In: Buccafusco JJ, editor. Methods of Behavior Analysis in Neuroscience. 2nd edition. Boca Raton (FL): CRC Press/Taylor & Francis. Chapter 5.
68. Jones EG, Huntley GW, and Benson DL (1994). Alpha calcium/calmodulin-dependent protein kinase II selectively expressed in a subpopulation of excitatory neurons in monkey sensory-motor cortex: comparison with GAD-67 expression. J. Neurosci 14, 611–629. doi:10.1523/JNEUROSCI.14-02-00611.1994. [PubMed: 8301355]
69. Erlander MG, Tillakaratne NJ, Feldblum S, Patel N, and Tobin AJ (1991). Two genes encode distinct glutamate decarboxylases. Neuron 7, 91–100. doi: 10.1016/0896-6273(91)90077-d. [PubMed: 2069816]
70. Cahoy JD, Emery B, Kaushal A, Foo LC, Zamanian JL, Christopherson KS, Xing Y, Lubischer JL, Krieg PA, Krupenko SA, et al. (2008). A transcriptome database for astrocytes, neurons, and oligodendrocytes: a new resource for understanding brain development and function. J. Neurosci 28, 264–278. doi: 10.1523/JNEUROSCI.4178-07.2008. [PubMed: 18171944]
71. Newman PJ, Berndt MC, Gorski J, White GC 2nd, Lyman S, Paddock C, and Muller WA. (1990). PECAM-1 (CD31) cloning and relation to adhesion molecules of the immunoglobulin gene superfamily. Science 247, 1219–1222. doi: 10.1126/science.1690453. [PubMed: 1690453]
72. Gothel SF, and Marahiel MA (1999). Peptidyl-prolyl cis-trans isomerases, a superfamily of ubiquitous folding catalysts. Cell Mol. Life Sci 55, 423–436. doi: 10.1007/s000180050299. [PubMed: 10228556]
73. Pavelka MS Jr., Weisbrod TR, and Jacobs WR Jr. (1997). Cloning of the dapB gene, encoding dihydrodipicolinate reductase, from Mycobacterium tuberculosis. J. Bacteriol 179, 2777–2782. doi: 10.1128/jb.179.8.2777-2782.1997. [PubMed: 9098082]
74. Bowyer JF, Thomas M, Patterson TA, George NI, Runnells JA, and Levi MS (2012). A visual description of the dissection of the cerebral surface vasculature and associated meninges and the choroid plexus from rat brain. J Vis Exp 69, e4285. doi: 10.3791/4285.
75. Guez-Barber D, Fanous S, Harvey BK, Zhang Y, Lehrmann E, Becker KG, Picciotto MR, and Hope BT (2012). FACS purification of immunolabeled cell types from adult rat brain. Journal of neuroscience methods, 203(1), 10–18. doi: 10.1016/j.jneumeth.2011.08.045. [PubMed: 21911005]
76. Abraham J, Prajapati SI, Nishijo K, Schaffer BS, Taniguchi E, Kilcoyne A, McCleish AT, Nelon LD, Giles FG, Efstratiadis A, et al. (2011). Evasion mechanisms to Igf1r inhibition in rhabdomyosarcoma. Mol. cancer therapeutics 10, 697–707. doi: 10.1158/1535-7163.MCT-10-0695.
77. Sokolov BP, Ala-Kokko L, Dhulipala R, Arita M, Khillan JS, and Prockop DJ (1995). Tissue-specific expression of the gene for type I procollagen (COL1A1) in transgenic mice. Only 476 base pairs of the promoter are required if collagen genes are used as reporters. The Journal of biological chemistry 270, 9622–9. doi: 10.1074/jbc.270.16.9622. [PubMed: 7721894]
78. Wang HY, Hsieh PF, Huang DF, Chin PS, Chou CH, Tung CC, Chen SY, Lee LJ, Gau SS, and Huang HS (2015). RBFOX3/NeuN is Required for Hippocampal Circuit Balance and Function. Scientific reports, 5, 17383. doi: 10.1038/srep17383. [PubMed: 26619789]
79. Pandey K, Yu XW, Steinmetz A, and Alberini CM (2021). Autophagy coupled to translation is required for long-term memory. Autophagy 17, 1614–1635. doi: 10.1080/15548627.2020.1775393. [PubMed: 32501746]
80. Ragan T, Kadiri LR, Venkataraju KU, Bahlmann K, Sutin J, Taranda J, Arganda-Carreras I, Kim Y, Seung HS, and Osten P (2012). Serial two-photon tomography for automated ex vivo mouse brain imaging. Nat. Methods 9, 255–258. doi: 10.1038/nmeth.1854. [PubMed: 22245809]
81. Wallrafen R, and Dresbach T (2018). The Presynaptic Protein Mover Is Differentially Expressed Across Brain Areas and Synapse Types. Frontiers in neuroanatomy 12, 58. doi: 10.3389/fnana.2018.00058. [PubMed: 30057527]
82. Winkler EA, Bell RD, and Zlokovic BV (2010). Pericyte-specific expression of PDGF beta receptor in mouse models with normal and deficient PDGF beta receptor signaling. Mol. Neurodegener 5:32. doi: 10.1186/1750-1326-5-32. [PubMed: 20738866]
83. Radu M, and Chernoff J (2013). An in vivo assay to test blood vessel permeability. J. Vis. Exp 73:e50062. doi: 10.3791/50062.

Author Manuscript Author Manuscript Author Manuscript Author Manuscript

Highlights

- Hippocampal *Igf2* is predominantly in pericytes where it increases following learning
- The learning-dependent pericytic *Igf2* increase requires neuronal activity
- IGF2 from pericytes, not fibroblasts or neurons, is required for long-term memory
- Pericytic IGF2 controls the increase of neuronal plasticity proteins upon learning

Author Manuscript Author Manuscript Author Manuscript Author Manuscript

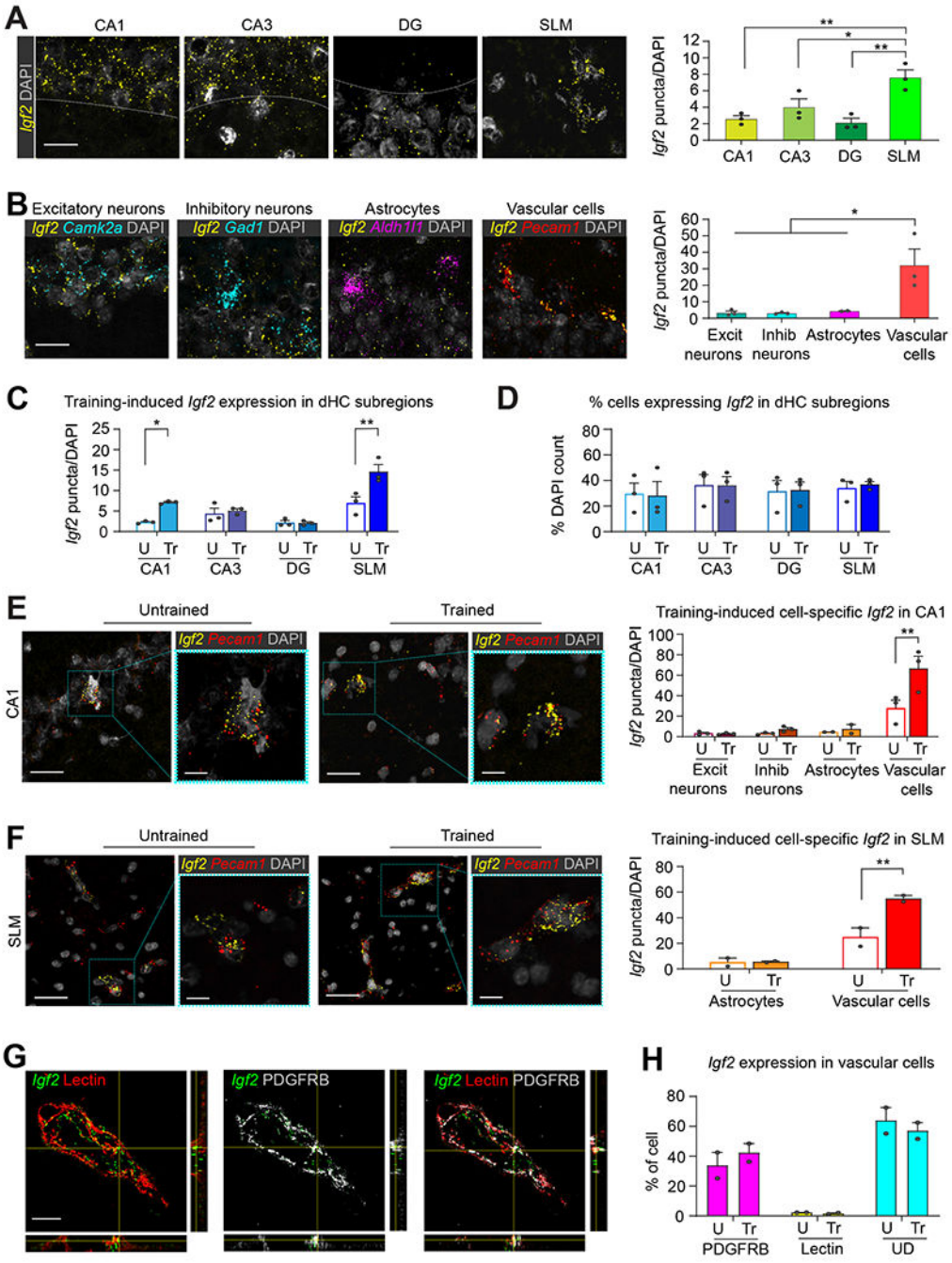

Figure 1: Subregion and cell type-specific distribution of basal and training-induced *Igf2* mRNA in rat dorsal hippocampus.

(A) Representative confocal images (scale bar 25 μm) and quantifications of *Igf2* RNAscope signal in the CA1, CA3, DG, and SLM/*stratum moleculare* layer of DG (SLM) subregions of dHC **(B)** Representative confocal images (scale bar 25 μm) and quantifications of *Igf2* RNAscope signal colocalized with cell-specific markers for excitatory (*Camk2a*) and inhibitory (*Gad1*) neurons, astrocytes (*Aldh1l1*), and vascular cells (*Pecam1*) in CA1. n = 3 rats, 14–66 images/subregion/rat. One-way ANOVA followed by Tukey's post hoc

Author Manuscript Author Manuscript Author Manuscript Author Manuscript

test. **(C)** Quantification of *Igf2* expression by dHC subregions in rats trained in inhibitory avoidance (Tr) and euthanized 20 h later. Control untrained rats (U) were left in their homecages and euthanized at matched time point. n = 3 rats/group, 14-66 images/subregion/group. **(D)** Percentage of *Igf2*-expressing cells in dHC subregions. n=3 rats/group, 10-46 images/subregion/group. **(E and F):** On the left, representative confocal images (scale bar 25 μm), higher magnification images (scale bar 10 μm) andon the right bar graph showing the quantification of *Igf2* expression by cell-type in **(E)** CA1 and **(F)** SLM. n = 3 rats/group. CA1: 14-15 images/rat/group; SLM: 4-6 images/rat/group. **(G)** Representative zoomed confocal images (scale bar: 15 μm) and orthogonal projections showing RNAscope-visualized *Igf2* mRNA puncta (green) colocalized with lectin (endothelial cells; red), PDGFRB (pericytes; white), or both. **(H)** Percentage of *Igf2* puncta colocalized with PDGFRB, lectin, or undetermined (UD). n=2 rats/group, 2 images/brain section, 2 brain sections/rat. Dots on graphs represent the number of puncta normalized to the total DAPI count for each rat. Data are shown as means ± s.e.m. Mixed-effects analyses followed by Bonferroni's multiple comparison tests. * $p < 0.05$, ** $p < 0.01$. Numeric values and detailed statistical analyses are reported in Table S1. Probes for RNAscope in Table S2. Markers for excitatory neurons: CamKIIα inhibitor neurons: Gad1; astrocytes: Aldh1l1; vascular cells: Pecam1; pericytes, smooth muscle cells and fibroblasts: PDGRFB; endothelial cells: Lectin.

Author Manuscript Author Manuscript Author Manuscript Author Manuscript

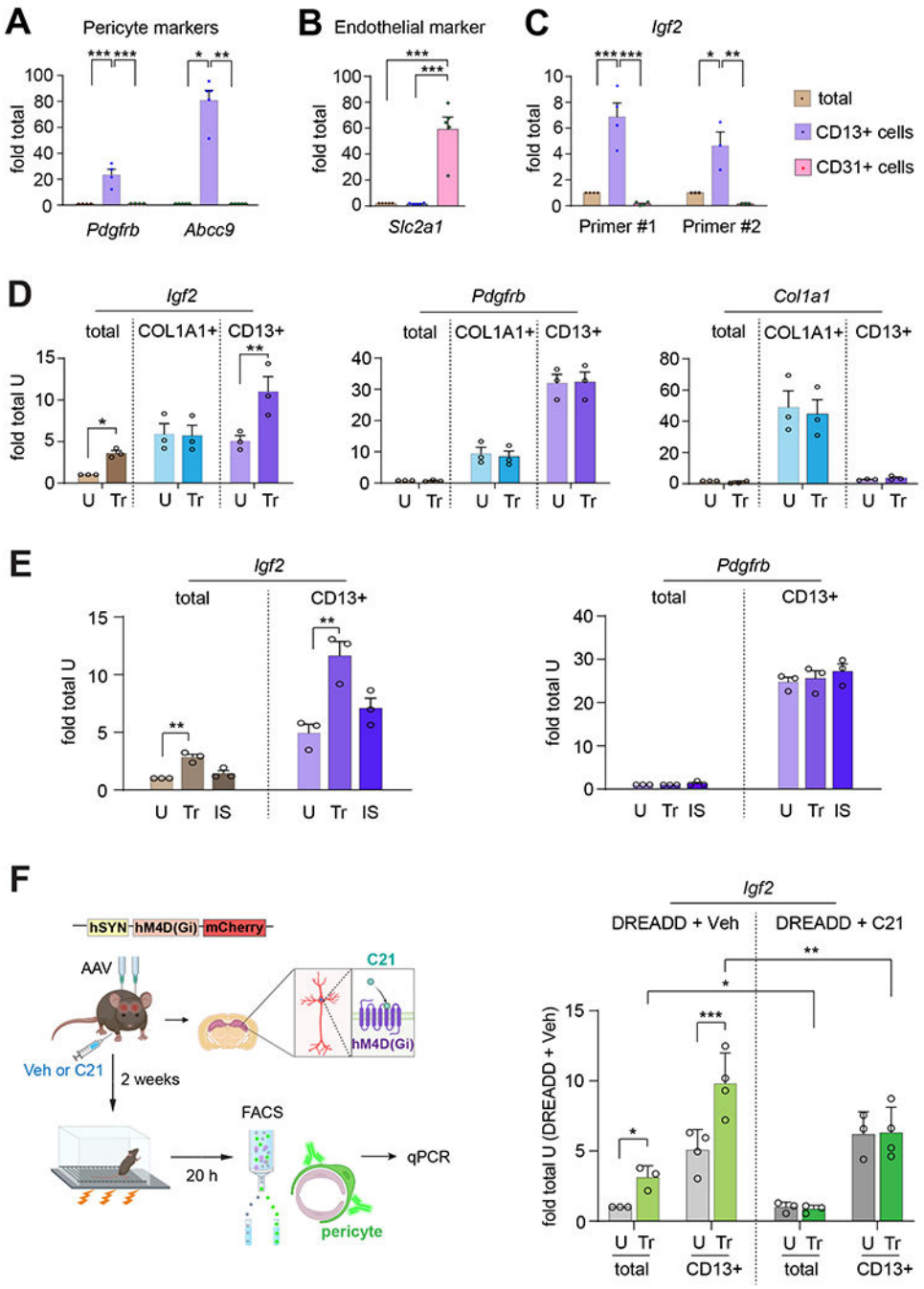

Figure 2: Learning significantly increases IGF2 expression in the hippocampal pericytes; this increase requires neuronal activity.

qPCR validation of the expression of **(A)** the pericyte markers *Pdgfrb* and *Abcc9* and **(B)** the endothelial marker *Slc2a1*, in RNA extracts from dHC (total) and FACS-purified CD13+ (pericytes) and CD31+ (endothelial) cells of mice. **(C)** qPCR of *Igf2* expression using two different primers (described in Table S3) in RNA extracts from dHC and FACS-purified CD13+ and CD31+ cells. Data are shown as fold change relative to the mRNA levels present in the dHC extract (dHC total); n = 4 mice/group per experiment,

Author Manuscript Author Manuscript Author Manuscript Author Manuscript

4 independent experiments. Dots on graphs represent value for each experiment. One-way ANOVA followed by Tukey's post hoc test. **(D)** qPCR analyses of *Igf2, Pdgfrb*, and Col1a1 expression in RNA extracts from dHC (total) and FACS-purified CD13+ (pericytes) and COL1A1+ (fibroblasts) of mice trained in CFC (Tr) and euthanized 20 h later. Control untrained mice (U) were left in their home cages and euthanized at matched timepoint. Data are shown as fold change relative to the mRNA levels present in the dHC extract (total) of untrained mice (U). n = 4 mice/group per experiment, 3 independent experiments. Dots on graphs represent the individual value for each experiment. Two-way ANOVA followed by Tukey's post hoc test. **(E)** qPCR analyses of *Igf2* and *Pdgfrb* mRNA levels in extracts from dHC (total) and FACS-purified CD13+ (pericytes) taken from the dHC of mice that underwent either CFC training (Tr) or an immediate shock (IS) and were euthanized 20 h later. Control untrained mice (U) were left in their homecages and euthanized at matched timepoint. Data are shown as fold change relative to the mRNA levels present in the dHC extract (total) of untrained mice. n=2-3 mice/group per experiment, 3 independent experiments. Dots on graph represent the individual value of each experiment. Two-way ANOVA followed by Tukey's post-hoc test. **(F)** Left panel: Experimental Design. Mice were bilaterally injected in the dHC with AAV8/hSyn-hM4D(Gi)-mCherry (DREADD); 2 weeks later the mice were injected i.p. with compound C21 (C21) or vehicle (Veh) and, 30 minutes later, trained in CFC, and, finally, euthanized 20 h after training. Control untrained mice (U) were left in their homecages and euthanized at matched time point. Right panel: Bargraph showing the *Igf2* mRNA levels in the RNA extracts from dHC (total) and FACS-purified CD13+ (pericytes) of mice expressing DREADD and injected with either Veh or C21. Data are shown as fold change relative to the mRNA levels present in the dHC extract (total) of untrained mice expressing DREADD and injected with Veh (U, DREADD + Veh). n = 2-3 mice/group per experiment, 3-4 independent experiments. Dots on graphs represent the individual value for each experiment. Three-way ANOVA followed by Tukey's post-hoc test. * $p < 0.05$, ** $p < 0.01$, *** $p < 0.001$. Numeric values and detailed statistical analyses are reported in Table S1. Primers for qPCR in Table S3. Markers for pericytes: Pdgfrb, Abcc9, CD13; markers for endothelial cells: Slc2a1, CD31; fibroblasts: Col1a1, Pdgfrb; smooth muscle cells: Pdgfrb.

Author Manuscript Author Manuscript Author Manuscript Author Manuscript

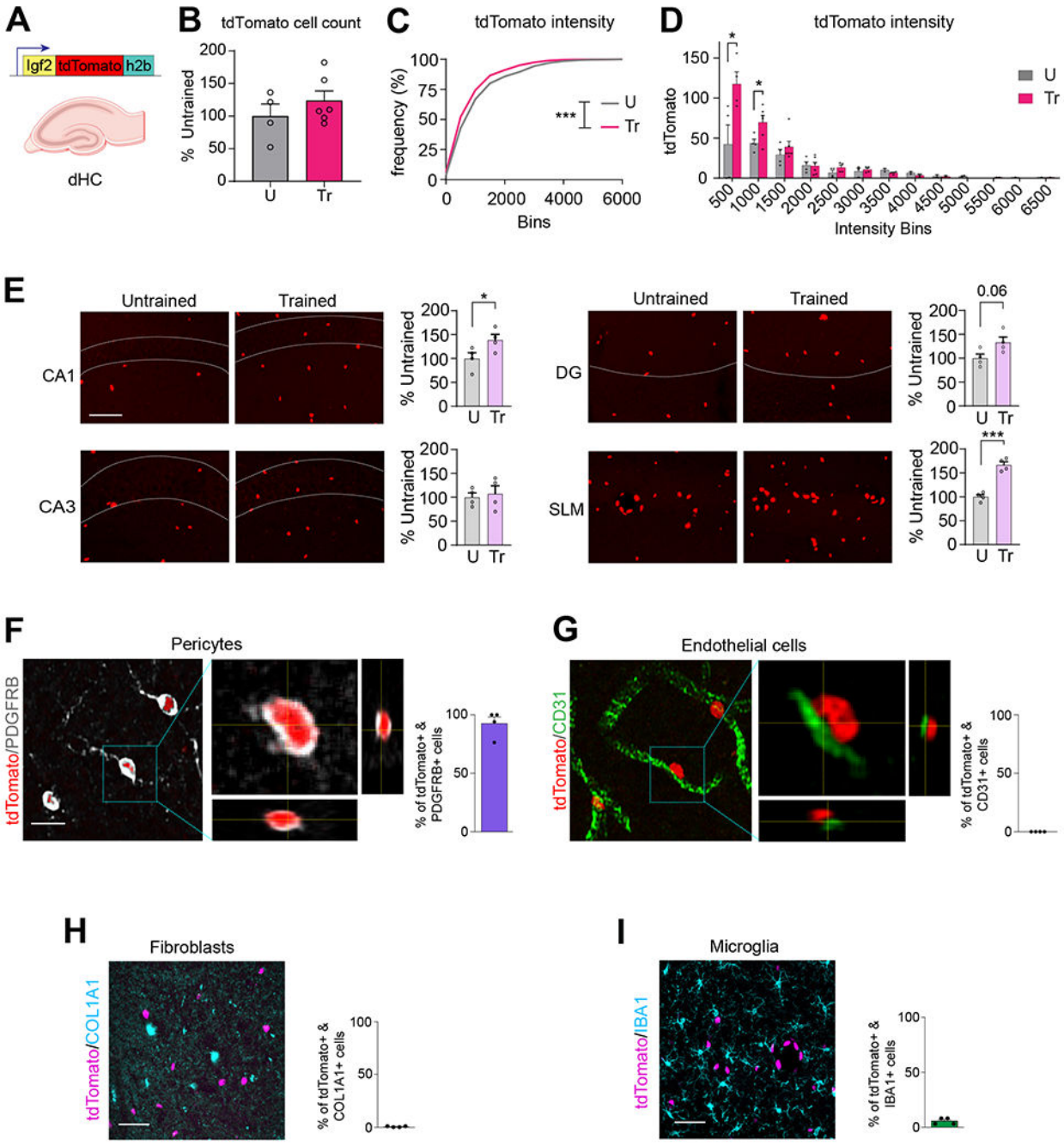

Figure 3: IGF2 is expressed in pericytes of mouse hippocampus, not in endothelial cells or fibroblasts.

(A) Schematic representation of the *Igf2* promoter-driven tdTomato-h2b construct. **(B)** Quantification of the number of tdTomato-labeled nuclei in the dHC from untrained (U) and CFC-trained (Tr) mice, normalized to the total DAPI count. Data are expressed as mean percent ± s.e.m. of untrained (U, 100%) mice, n = 4-6 mice/group, 12 images/mouse. Dots on graph represent the mean value for each mouse. Unpaired t-test. **(C)** Relative frequency distribution of cells showing tdTomato fluorescence intensity in the dHC of

Author Manuscript Author Manuscript Author Manuscript Author Manuscript

untrained (U) and CFC-trained (Tr) mice. n = 4–6 mice/group, 3 brain sections/mouse, 4 images/brain section. Kolmogorov–Smirnov test for cumulative distribution of U and Tr data points, p = 0.0002. **(D)** Binned tdTomato fluorescence intensity in U and Tr animals. Data are expressed as mean ± s.e.m. Dots on graphs represent the summed values for all brain sections from each mouse. Unpaired t-test between U and Tr within each intensity bin. **(E)** Representative confocal images (scale bar: 20 μm) and quantifications of tdTomato-labeled nuclei from CA1, CA3, DG and SLM in untrained (U) and CFC-trained (Tr) IGF2-tdTomato-H2B mice. Data are expressed as percent of tdTomato positive cells ± s.e.m. normalized to the total DAPI count relative to untrained (U, 100%) mice, n = 3 mice/group. Dots on graphs represent the value for each mouse. Unpaired t-test. * $p < 0.05$, ** $p < 0.01$, *** $p < 0.001$. **(F, G)** Representative confocal images and relative quantifications showing percentage of tdTomato-labeled nuclei colocalized with (**F**) PDGFRB-positive cells (pericytes) and (**G**) CD31-positive cells (endothelial cells) in the SLM/*stratum moleculare* along with orthogonal projections showing tdTomato-labeled nuclei and immunopositive cells (scale bar, 15 μm). **(H, I)** Representative confocal images of SLM/*stratum moleculare* (scale bar: 50 μm) and relative quantifications showing percentage of tdTomato-labeled nuclei colocalized with (**H**) COL1A1-positive (fibroblasts) or **(I)** IBA1-positive (microglia) cells. Data are expressed as % mean ± s.e.m. of doubly positive cells relative to the total number of tdTomato-labeled nuclei (100%); n = 4 mice/group. Numeric values and detailed statistical analyses are reported in Table S1. Markers for endothelial cells: CD31; pericytes: PDGFRB; fibroblasts COL1A1; microglia: IBA1.

Author Manuscript Author Manuscript Author Manuscript Author Manuscript

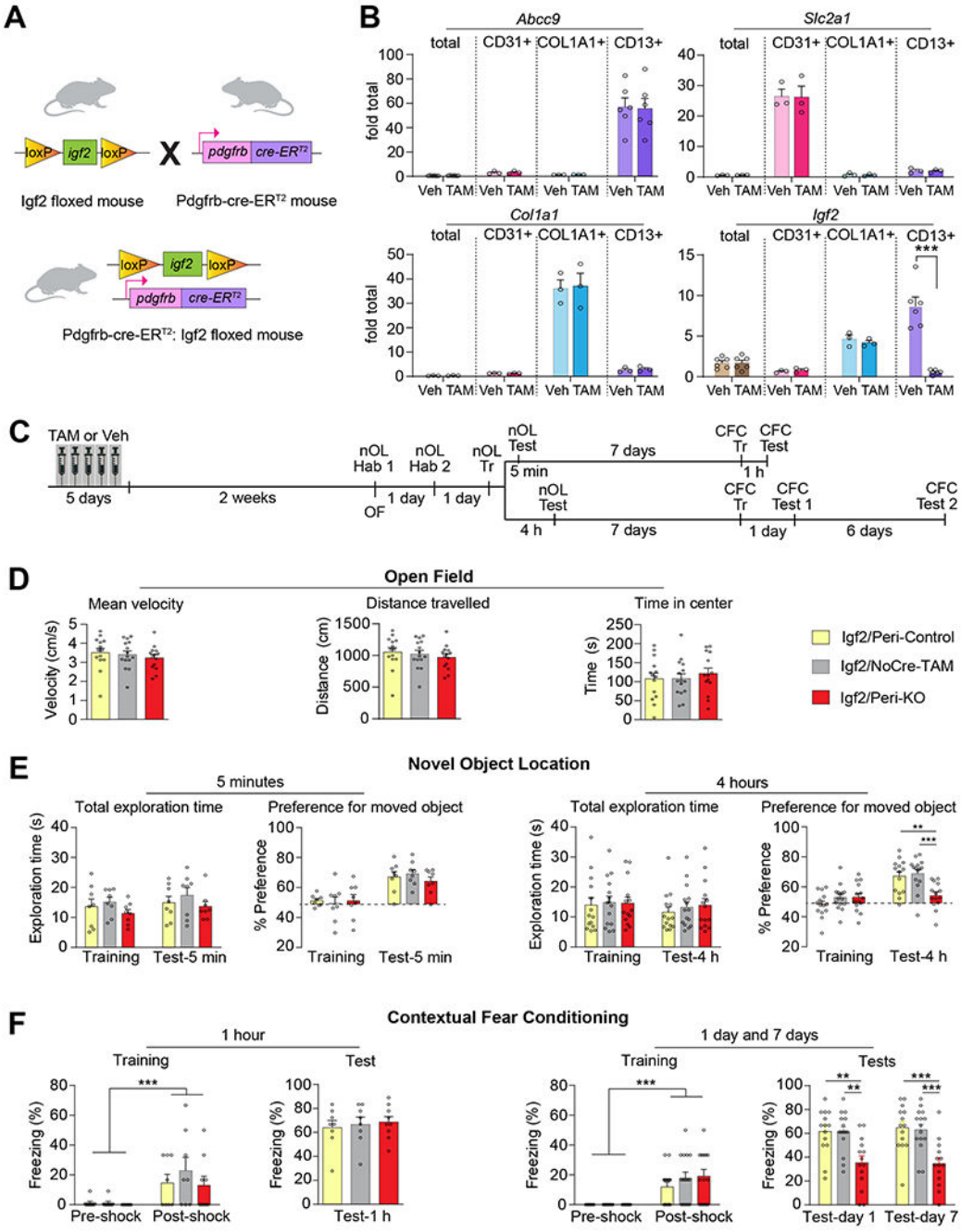

Figure 4: Pericyte-specific KO of *Igf2* impairs novel object location and contextual fear memories.

(A) Pdgfrb-Cre-ER^{T2}:Igf2 floxed mice were generated by breeding *Igf2* floxed mice and Pdgfrb-Cre-ER^{T2} mice. **(B)** qPCR analyses of *Abcc9, Slc2a1, Col1a1* and *Igf2* mRNA in RNA extracts from dHC (total) and FACS-purified CD13+ (pericytes), CD31+ (endothelial cells), COL1A1+ (fibroblasts) and CD13+ (pericytes) of tamoxifen (TAM)- or vehicle (Veh)-injected PDGFB-Cre *Igf2*-floxed mice. Data are shown as fold change relative to the mRNA levels present in the the dHC extract of Veh-injected PDGFRB-Cre *Iqf2*-floxed

Author Manuscript Author Manuscript Author Manuscript Author Manuscript

mice (Veh, dHC total); n = 3 mice/group per experiment, 3 independent experiments. Dots on graphs represent value for each experiment. Two-way ANOVA followed by Tukey's post-hoc test. **(C)** Experimental schedule of behaviors on Igf2/Peri-KO, Igf2/Peri-Control, and Igf2/NoCre-TAM mice. **(D)** Open field test, expressed as average velocity (cm/s), total distance traveled (cm), and time spent in the center of arena (s). n = 14–15 mice/group. One-way ANOVA followed by Bonferroni's post-hoc test. **(E)** Total exploration times and novel object location (nOL) memory tested at 5 minutes (left panels) or 4 hours (right panels) after training. nOL memory is expressed as mean percent preference ± s.e.m. for the displaced object. **(F)** CFC training and memory tested at 1 hour (left panels), and 1 day and 7 days (right panels) after training. CFC memory was expressed as mean percent freezing ± s.e.m. n = 8–15 mice/group. Two-way RM ANOVA followed by Bonferroni's post-hoc test. Dots on graphs represent the value for each mouse. ** $p < 0.01$, *** $p < 0.001$. Numeric values and detailed statistical analyses are reported in Table S1. Primers for qPCR in Table S3. Markers for endothelial cells: Slc2a1 and CD31; pericytes: Abcc9 and CD13; fibroblasts: Col1a1.

Author Manuscript Author Manuscript Author Manuscript Author Manuscript

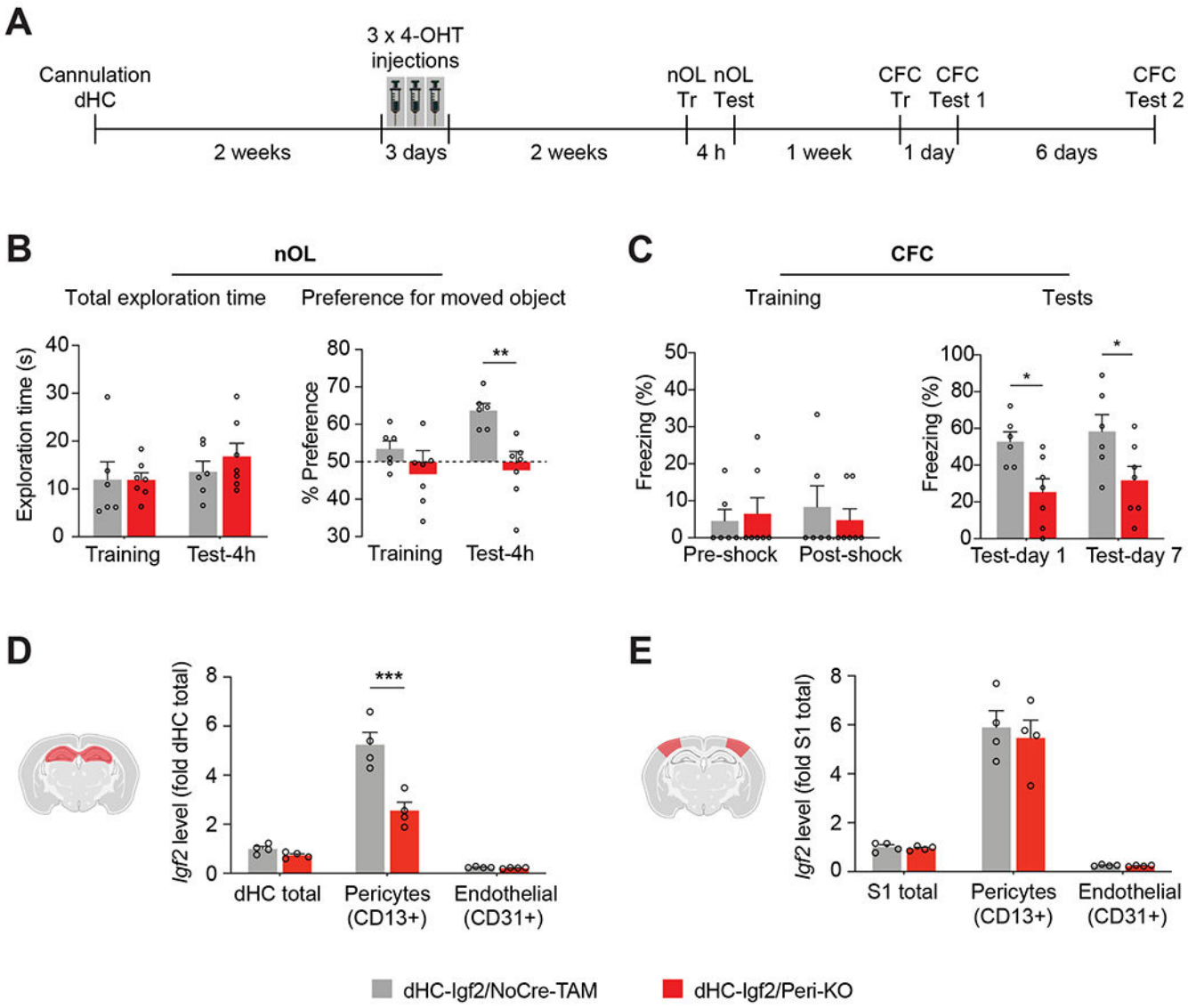

Figure 5: *Igf2* knockout in dHC pericytes impairs novel object location and contextual fear memories.

(A) Experimental schedule. DHC-Igf2/Peri-KO and dHC-Igf2/NoCre-TAM were assessed for **(B)** Total exploration time (left panel), and preference for the moved object (right panel) tested 4 hours after nOL training; nOL memory is expressed as mean percent preference ± s.e.m. for the moved object. **(C)** CFC training (left panel) and memory tested (right panel) at 1 and 7 days after training. CFC memory is expressed as mean percent freezing ± s.e.m. For **B** and **C**, n = 6–7 mice/group, 2 independent experiments. Dots on graphs represent the value for each mouse. Two-way RM ANOVA followed by Bonferroni's post-hoc test. **(D, E)** qPCR analyses of *Igf2* mRNA levels in dHC and primary somatosensory cortex (S1), and FACS-purified CD13+ (pericytes) and CD31+ (endothelial cells) from both regions. Data are expressed as fold change ± s.e.m. relative to the mRNA levels of dHC (dHC total) and S1 (S1 total); n = 4 mice/group per experiment, 4 independent experiments. Dots on graphs represent value for each experiment. Two-way ANOVA followed by Bonferroni's post-hoc

Author Manuscript Author Manuscript Author Manuscript Author Manuscript

test. * $p < 0.05$, ** $p < 0.01$, *** $p < 0.001$. Numeric values and detailed statistical analyses are reported in Table S1. Primers for qPCR in Table S3. Marker for endothelial cells: CD31; pericytes: CD13.

Author Manuscript Author Manuscript Author Manuscript Author Manuscript

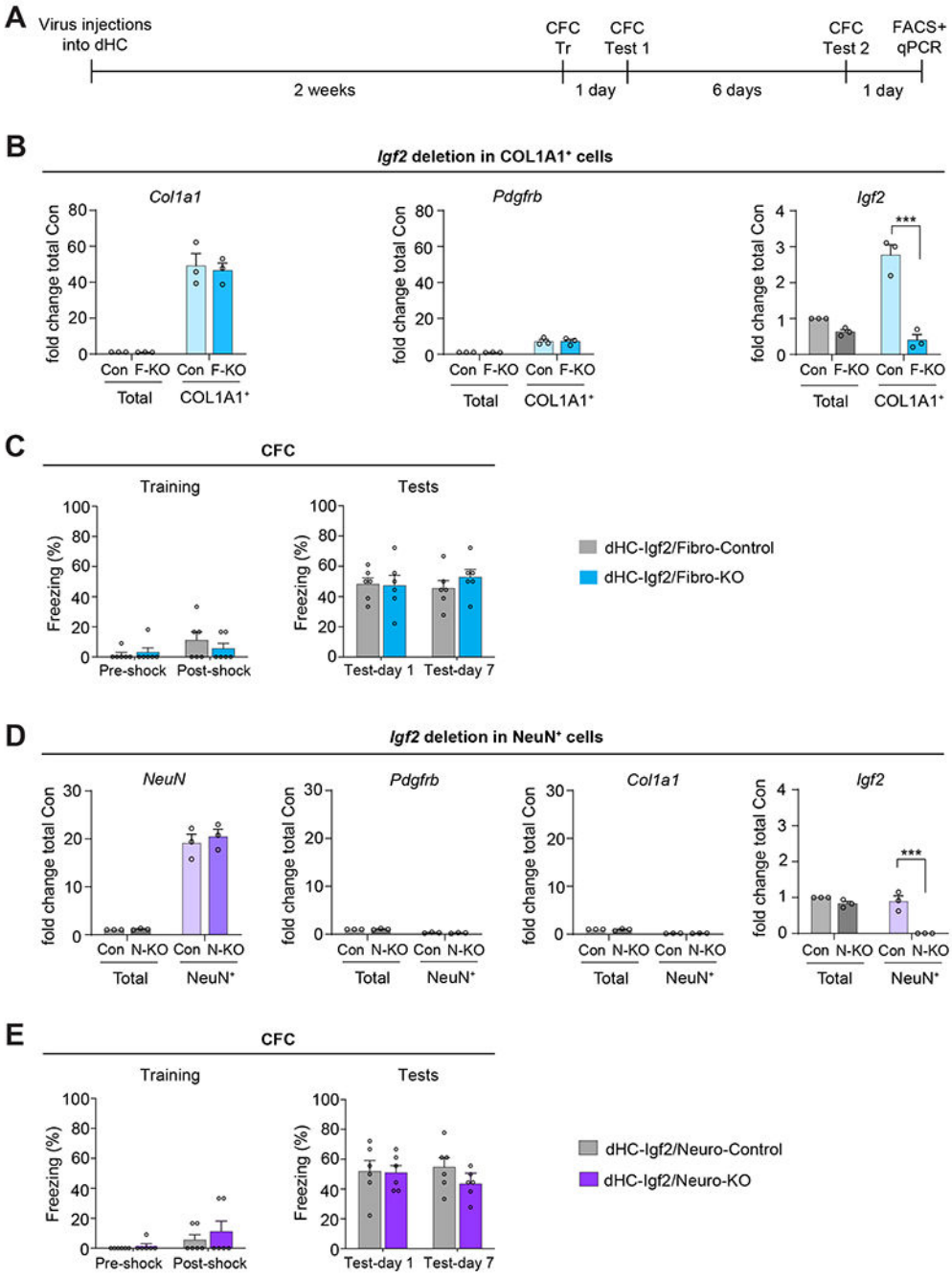

Figure 6: *Igf2* knockout in dHC fibroblasts or neurons does not affect contextual fear memory.

(A) Experimental schedule. Fibroblast or neuron-specific Igf2 deletion was induced in *Igf2*-floxed mice by injecting into their dHC a virus expressing Cre-recombinase under the *Col1a1* promoter to target fibroblasts [(dHC-Igf2/Fibro-KO or F-KO) or GFP (dHC-Igf2/Fibro-Control or Con) sequence)], or under *hSyn* promoter to target neurons [(dHC-Igf2/Neuro-KO or N-KO) or GFP (dHC-Igf2/Neuro-Control or Con)]. **(B)** qPCR analyses of *Col1a1, Pdgfrb*, and *Igf2* mRNA from dHC (total) and FACS-purified COL1A1+ cells (fibroblasts) from dHC-Igf2/Fibro-KO or dHC-Igf2/Fibro-Control mice. Data are shown

Author Manuscript Author Manuscript Author Manuscript Author Manuscript

as fold change relative to the mRNA levels of the dHC (total) extract obtained from dHC-Igf2/Fibro-Control mice (Con, Total). n = 2-3 mice were pooled in each experiment, 3 independent experiments. Dots on graphs represent the value for each experiment. Two-way ANOVA followed by Sidak's post-hoc test. *** $p < 0.001$. **(C)** CFC training (left panel) and memory tested at 1 and 7 days after training (right panel). CFC memory is expressed as mean percent freezing ± s.e.m; n = 6 mice/group, 2 independent experiments. Dots on graphs represent the value for each mouse. Two-way RM ANOVA followed by Bonferroni's post-hoc test. **(D)** qPCR analyses of *NeuN, Pdgfrb, Col1a1*, and *Igf2* mRNA in the RNA extracts from dHC (total) and FACS-purified NeuN+ cells (neurons) of dHC-Igf2/Neuro-KO or dHC-Igf2/Neuro-Control mice. Data are shown as fold change relative to the mRNA levels in the dHC (total) extract obtained from dHC-Igf2/Neuro-Control mice (Con, Total); n = 2-3 mice pooled in each experiment, 3 independent experiments. Dots on graphs represent the value for each experiment. Two-way ANOVA followed by Sidak's post-hoc test. *** $p < 0.001$. **(E)** CFC training (left panel) and memory tested at 1 and 7 days after training (right panel). CFC memory is expressed as mean percent freezing ± s.e.m; n = 6 mice/group, 2 independent experiments. Dots on graphs represent the value for each mouse. Two-way RM ANOVA followed by Bonferroni's post-hoc test. Numeric values and detailed statistical analyses are reported in Table S1. Primers for qPCR in Table S3. Markers for fibroblasts Col1a1 and Pdgfrb; neurons: NeuN; pericytes: Pdgfrb.

Author Manuscript Author Manuscript Author Manuscript Author Manuscript

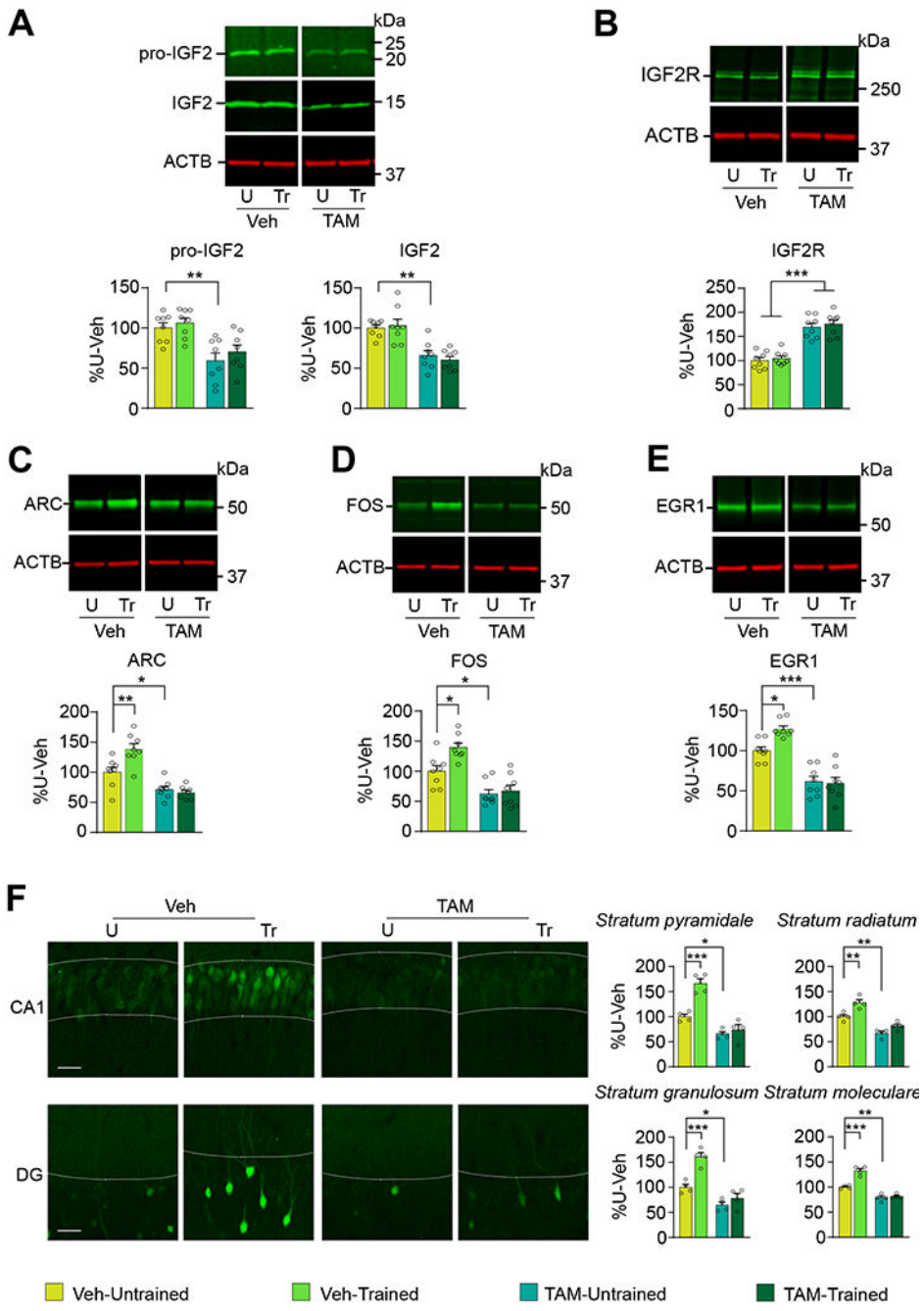

Figure 7. Pericyte-specific ablation of IGF2 significantly decreases levels of pro-IGF2, IGF2, and immediate early genes, but increases the level of IGF2R.

PDGFB-Cre *Igf2*-floxed mice were injected *i.p.* with tamoxifen (TAM) or vehicle (Veh), one injection per day for 5 consecutive days. Two weeks later, mice were trained (Tr) in CFC and euthanized 1 hour later. Control untrained mice (U) were left in their home cages and euthanized at matched timepoints. Representative western blots and relative densitometric analyses of **(A)** pro-IGF2 and IGF2, **(B)** IGF2 receptor (also known as cation-independent mannose-6-phosphate receptor; CIM6PR), **(C)** ARC, **(D)** FOS, and **(E)** EGR1

Author Manuscript Author Manuscript Author Manuscript Author Manuscript

in dHC extracts. ACTB was used as a control for equal loading. Data are expressed as percent (%) mean ± s.e.m of vehicle-injected untrained mice (% U-Veh). n = 8 mice/group, 2 independent experiments. **(F)** Representative confocal images (scale bar: 20 μm) and quantifications of ARC immunofluorescence intensities in CA1 *stratum pyramidale* (s.p.) and *stratum radiatum* (s.r.) layers, and DG *stratum granulosum* (s.g.) and *stratum moleculare* (s.m.) layers of tamoxifen (TAM) or vehicle (Veh)-injected PDGFB-Cre *Igf2*-floxed mice untrained (U) or trained in CFC (Tr). Data are expressed as % mean ± s.e.m of vehicle-injected untrained mice (% U-Veh). n = 4 mice per group, 2 independent experiments. Two-way ANOVA followed by Tukey's post-hoc test. Dots on graphs represent the value for each mouse. * $p < 0.05$, ** $p < 0.01$, *** $p < 0.001$. Numerical values and detailed statistical analyses are reported in Table S1.

Author Manuscript Author Manuscript Author Manuscript Author Manuscript

Key resources table

REAGENT or RESOURCE	SOURCE	IDENTIFIER
Antibodies		
anti-PDGFRB	R&D Systems	Cat# AF1042 RRID:AB_2162633
anti-Collagen1	Thermo Fisher Scientific	Cat# 600-402-103 RRID:AB_2614800
anti-CD13	BD Pharmingen	Cat# 558744 RRID:AB_397101
anti-COL1A1	Invitrogen	Cat # MA5-43886 RRID:AB_2912818
anti-CD31	BD Pharmingen	Cat# 557355 RRID:AB_396660
anti-IBA1	Fujifilm Wako Chemicals	Cat# 019-19741 RRID:AB_839504
anti-NeuN	Millipore Sigma	Cat# MAB377 RRID:AB_2298772
anti-IGF2 receptor	Abcam	Cat# ab262713 RRID:AB_2936901
anti-IGF2	Abcam	Cat# ab9574 RRID:AB_308725
anti-cation independent mannose 6 phosphate receptor	Abcam	Cat# ab124767 RRID:AB_10974087
anti-Arc	Synaptic Systems	Cat# 156003 RRID:AB_887694
anti-c-Fos	Cell Signaling Technology	Cat# 2250 RRID:AB_2247211
anti-EGR1	Cell Signaling Technology	Cat# 4153 RRID:AB_2097038
Donkey anti-goat Alexa Fluor 647	Invitrogen	Cat# A21447 RRID:AB_141844
Goat anti-rabbit Alexa Fluor 647	Invitrogen	Cat# A21244 RRID:AB_2535812
Donkey anti-rat Alexa Fluor 488	Invitrogen	Cat# A21208 RRID:AB_2535794
Goat anti-rabbit Alexa Fluor 488	Invitrogen	Cat# A11034 RRID:AB_2576217
Goat anti-rabbit Alexa Fluor 568	Invitrogen	Cat# A11036 RRID:AB_10563566
Dylight 594 Lycopersicon esculentum (Tomato) lectin	Vector Laboratories	Cat# DL-1177 RRID:AB_2336416
Goat anti-mouse IRdye680LT	LI-Cor Bioscience	Cat# 926-68020 RRID:AB_10706161
Goat anti-rabbitIRdye800CW	LI-Cor Bioscience	Cat# 926-32211 RRID:AB_621843
anti-Actin	Santa Cruz Biotechnology	Cat# sc-47778 RRID:AB_626632
Bacterial and virus strains		
AAV8/hSyn-mCherry	Addgene	Cat# 114472
AAV8/hSyn-hM4Di-mCherry	Addgene	Cat# 50475

Author Manuscript Author Manuscript Author Manuscript Author Manuscript

REAGENT or RESOURCE	SOURCE	IDENTIFIER
LV/Col1a1-Cre-EGFP	Vector Builder	
LV/Col1a1-EGFP	Vector Builder	
AAV8/hSyn-Cre-EGFP	Addgene	Cat# 105540
AAV8/hSyn-EGFP	Addgene	Cat# 50465
Chemicals, peptides, and recombinant proteins		
Tamoxifen	Sigma-Aldrich	Cat# T5648
4-hydroxytamoxifen (4-OHT)	Sigma-Aldrich	Cat# H6278
Pretreatment 4 solution	ACD	Cat# 320513
RNAscope® 2.5 Fluorescent Multiplex Kit	ACD	Cat # 320293
Compound 21	HelloBio	Cat# HB6124
ProLong™ Diamond Antifade Mountant	Life Technologies	Cat# P36961
ProLong™ Diamond Antifade Mountant with DAPI	Life Technologies	Cat# P36962
Ebioscience™ Intracellular Fixation & Permeabilization Buffer Set	Thermo Scientific	Cat# 88-8824-00
RNeasy Universal Plus Mini Kit	Qiagen	Cat# 73404
RNeasy Micro kit	Qiagen	Cat# 74004
QuantiTect Reverse Transcription Kit	Qiagen	Cat# 205311
iQ SYBR Green Supermix	Bio-Rad	Cat# 107-8882
DAPI	Thermo Scientific	Cat# 62247
Paraformaldehyde	Sigma	Cat# 158127
Lipopolysaccharide (LPS)	Sigma	Cat# L6011
Experimental models: Organisms/strains		
Adult C57BL6 mice	Jackson Laboratories	Stock #000664
Adult PDGFRB-P2A-CreERT2 mice	Jackson Laboratories	Stock #030201
Adult Igf2-floxed mice	Kindly provided by Drs. Miguel Constancia and Ionel Sandovici, University of Cambridge	
Adult IGF2-tdTomato-H2B mice	Kindly provided by Cold Spring Harbor Laboratories (CSHL)	
Adult male Long Evans rats	Envigo	Order code: 140
Software and algorithms		
Image J	Schneider et al., 2012	https://imagej.nih.gov/ij/
Prism 7	GraphPad Software Inc.	
EthoVision-XT13	Noldus	